ANL/RAS 75-39

AN IMPLICIT THREE-DIMENSIONAL FINITE-ELEMENT FORMULATION FOR THE NONLINEAR STRUCTURAL RESPONSE OF REACTOR COMPONENTS

R. F. Kulak and T. B. Belytschko*

September 1975

Reactor Analysis and Safety Division
ARGONNE NATIONAL LABORATORY
9700 South Cass Avenue
Argonne, Illinois 60439

* Department of Materials Engineering, University of Illinois, Chicago Circle

AN IMPLICIT THREE-DIMENSIONAL FINITE-ELEMENT FORMULATION FOR THE NONLINEAR STRUCTURAL RESPONSE OF REACTOR COMPONENTS

R. F. Kulak and T. B. Belytschko*

September 1975

Reactor Analysis and Safety Division
ARGONNE NATIONAL LABORATORY
9700 South Cass Avenue
Argonne, Illinois 60439

* Department of Materials Engineering, University of Illinois, Chicago Circle

TABLE OF CONTENTS

ABSTRACT

This report describes the formulation of a finite-element procedure for the implicit transient and static analysis of plate/shell type structures in three-dimensional space. The triangular plate/shell element can sustain both membrane and bending stresses. Both geometric and material nonlinearities can be treated, and an elastic-plastic material law has been incorporated. The formulation permits the element to undergo arbitrarily large rotations and translations; but, in its present form it is restricted to small strains.

The discretized equations of motion are obtained by a stiffness method. An implicit integration algorithm based on trapezoidal integration formulas is used to integrate the discretized equations of motion in time. To insure numerical stability, an iterative solution procedure with equilibrium checks is used.

I. INTRODUCTION

In assessing the safety of liquid-metal fast breeder reactors (LMFBRs), numerical structural analysis codes are needed for a large variety of time scales and geometries. In constructing models to represent realistic accident situations, it is imperative that the programs be capable of handling problems in three-dimensional space. A previously developed code called SADCAT (Ref. 1) partially fulfilled the above objectives, but was limited to relatively short time scales because of its explicit temporal integration. The present code is developed to augment SADCAT by adding implicit integration with long time capabilities so that together the two codes have the capability to treat the large variety of time scales which are found in LMFBR structural safety evaluations.

As mentioned before, the existing SADCAT code uses an explicit integration scheme which inherently necessitates the use of a small time step to maintain numerical stability. The use of a small time step restricts its application to loadings of relatively short duration and thus precludes the economic solution of long duration loadings and static problems.

The program described herein is based on an implicit-integration procedure and is developed to handle both long-duration dynamic problems and static problems. The method is formulated using corotational coordinate systems. The corotational coordinates facilitate the formulation of element related quantities. Argyris et al (Ref. 2) utilized corotational coordinates in static problems. The angular equations of motion are formulated in body coordinates which permit arbitrarily large rotations. The translational equations of motion are formulated in the global coordinate system.

The program has the same triangular plate/shell element as SADCAT; hence, the code is applicable to thin structures. The element is capable of sustaining both membrane and bending loads. In its present formulation, the element is able

to undergo arbitrarily large rotations and translations, but it is restricted to small strains. An elastic and elastic-plastic stress strain law with isotropic linear hardening and a Mises yield condition is included in the program, and other material laws can easily be added.

Because the code was developed to handle problems characterized by both geometric and material nonlinearities, an iterative-incremental solution procedure with equilibrium checks based on an energy balance is used. The code has the ability to internally adjust the time step or, in the case of static problems, the load increment when an equilibrium configuration cannot be attained.

II. DEVELOPMENT OF THE ANALYSIS

A. Coordinate Systems

The discretization of the continuous structure in space is accomplished by a finite element method. The structure is subdivided into a finite number of discrete triangular elements which can sustain both bending and membrane loads. This element is also used in the Argonne developed code SADCAT (Ref. 1).

For ease of formulation and solution three coordinate systems are used: corotational coordinates, body coordinates, and global coordinates. A unique set of corotational coordinates is associated with each triangular element. The use of these coordinates greatly simplifies the formulation of the deformation displacements, strain-displacement equations, and the stress-strain relationship. The corotation coordinate system has its origin at node 1 of each triangular element with the $\hat{x}$ and $\hat{y}$ axes lying in the plane formed by nodes 1, 2, and 3 (Fig. 1). The $\hat{x}$-axis bisects the angle α. A hat, $\hat{}$, above a quantity is herein used to indicate that the quantity is referred to the corotational coordinate system.

For the purpose of treating motion in which the nodal rotations are arbitrarily large, a set of unit vectors fixed to each node is used to describe its orientation. The unit vectors $\underline{b}_1$, $\underline{b}_2$, and $\underline{b}_3$ of each node coincide with the principal axes of the mass moments of inertia and define the orientation of the body coordinate system $(\bar{x},\bar{y},\bar{z})$, as shown in Fig. 1. A bar, $\bar{}$, above a quantity, indicates that it is referred to the body coordinate system. A global coordinate system (x,y,z) is fixed in space.

In the computation, it is necessary to transform quantities measured in one system into complementary quantities measured in another. To accomplish this, several coordinate transformation matrices are developed in Appendix A.

B. Equations of Motion

The translational equations of motion are

$$M_J \ddot{u}_{Ji} = f^{ext}_{Ji} - f^{int}_{Ji} \tag{1}$$

where

M_J = mass of node J

u_{Ji} = linear displacement of node J in the i^{th} direction

$f^{int}_{Ji}, f^{ext}_{Ji}$ = internal and external forces, respectively, at node J in the i^{th} direction.

The rotational equations, which are identical to the Euler equations, based upon an isotropic inertia tensor, are expressed in the moving body-coordinate system in the form

$$\bar{I}_{Jii}\bar{\alpha}_{Ji} = \bar{m}^{ext}_{Ji} - \bar{m}^{int}_{Ji} + \bar{\omega}_{Jj}\bar{\omega}_{Jk}(\bar{I}_{Jjj} - \bar{I}_{Jkk}) \tag{2}$$

where

$\bar{I}_{Jii}$ = mass moment of inertia of node J in the i^{th} body coordinate direction (a principal moment of inertia)

$\bar{m}^{int}_{Ji}, \bar{m}^{ext}_{Ji}$ = internal and external moments, respectively, at node J

$\bar{\omega}_{Ji}$ = i^{th} component of the angular velocity of node J measured in body coordinates

$\bar{\alpha}_{Ji}$ = i^{th} component of the angular acceleration of node J measured in body coordinates

i,j,k = $\bar{x},\bar{y},\bar{z}$ or any cyclic permutation

Because the code is being developed for the purpose of analyzing reactor components, such as hexcans which exhibit nonlinear material and/or geometric behavior under extreme loads, it is necessary to use an incremental form for the internal forces. The incremental expression for nodal internal forces are obtained as follows. Using the local-to-global transformation matrix, [T], the internal nodal forces for a generic element are given by

$$\{f^{int}\} = [T]\{\hat{f}^{int}\} \quad . \tag{3}$$

The increments in internal force for a generic element are obtained by subtracting Eq. 3 at time i from 3 at time i+1 to give

$$\{\Delta f^{int}\} = [T_{i+1}]\{f^{int}_{i+1}\} - [T_i]\{f^{int}_i\} \quad . \tag{4}$$

Expressing the quantities at time i+1 in terms of the quantities at time i, we obtain

$$[T_{i+1}] = [T_i] + [\Delta T] \tag{5}$$

and

$$\{f^{int}_{i+1}\} = \{f^{int}_i\} + \{\Delta f^{int}\} \quad . \tag{6}$$

Substituting Eqs. 5 and 6 into 4 and neglecting terms quadratic in increments we have, for an element,

$$\{\Delta^{int}_f\} = [T_i]\{\Delta f\} + [\Delta T]\{f_i\} \tag{7}$$

These two terms are well known in structural analysis and correspond to the linear tangential stiffness $[K_T]$ and "initial stress" or geometric stiffness $[K_G]$, respectively.

Using the latter nomenclature, we may write

$$\{\Delta f^{int}\} = [K_T]\{\Delta d\} + [K_G]\{\Delta d\} \tag{8}$$

The increment in internal forces expressed in the mixed coordinate system is obtained from

$$\{\Delta \tilde{f}^{int}\} = [\tilde{T}]\{\Delta f^{int}\} \tag{9}$$

The total increment in the global internal-force matrix is obtained by summing the contributions of all the elements, that is

$$\{\Delta \tilde{F}^{int}\} = \sum_{n=1}^{N} [L]^T_{(n)} \{\Delta \tilde{f}^{int}\}_{(n)} \tag{10}$$

where $[L]_{(n)}$ is a Boolean connectivity matrix (Oden, Ref. 3) and N is the total number of elements. Similarly, the total nodal internal force at the i^{th} step is given by

$$\{\tilde{F}_i^{int}\} = \sum_{n=1}^{N} [L]^T_{(n)} \{\tilde{f}_i^{int}\}_{(n)} \tag{11}$$

The total internal nodal force at the $i+1$ step is now equal to

$$\{\tilde{F}_{i+1}^{int}\} = \{\tilde{F}_i^{int}\} + \{\Delta \tilde{F}^{int}\} \tag{12}$$

Writing the equation of motion (Eq. 1) at time step $i+1$, we obtain

$$[\tilde{M}]\{\ddot{\tilde{d}}_{i+1}\} + \{\tilde{F}_i^{int}\} + \{\Delta \tilde{F}^{int}\} = \{\tilde{F}_{i+1}^{ext}\} \tag{13}$$

When the stress-strain law is linearized about the state of stress at the i^{th} time step, a linear equation for $\{\Delta\tilde{d}\}$ may be obtained

$$\{\Delta \tilde{F}^{int}\} \cong [\tilde{K}]\{\Delta \tilde{d}\} \tag{14}$$

where

$$[\tilde{K}] = [\tilde{K}_T] + [\tilde{K}_G]$$

$[\tilde{K}_T]$ = global tangential stiffness matrix

$[\tilde{K}_G]$ = geometric stiffness matrix

In view of the above approximations, the equation of motion becomes

$$[\tilde{M}]\{\ddot{\tilde{d}}_{i+1}\} + [\tilde{K}]\{\Delta\tilde{d}\} = \{\tilde{F}^{ext}_{i+1}\} - \{\tilde{F}^{int}_{i}\} \quad . \tag{15}$$

In order to develop an implicit algorithm it is necessary to express the kinematic quantities at the time step $i+1$ in terms of those at the i^{th} step. To accomplish this, the trapezoidal integration formulas (Ref. 4) are used. They are

$$\{\tilde{d}_{i+1}\} = \{\tilde{d}_i\} + \Delta t\{\dot{\tilde{d}}_i\} + \frac{1}{4}\Delta t^2[\{\ddot{\tilde{d}}_i\} + \{\ddot{\tilde{d}}_{i+1}\}] \tag{16}$$

and

$$\{\dot{\tilde{d}}_{i+1}\} = \{\dot{\tilde{d}}_i\} + \frac{\Delta t}{2}(\{\ddot{\tilde{d}}_i\} + \{\ddot{\tilde{d}}_{i+1}\}) \tag{17}$$

where Δt is the time step. This corresponds to a linear velocity and constant acceleration during the time interval. Using (16) and (17), the equations of motion become

$$\left[[\tilde{M}] + \Delta t^2\beta[\tilde{K}]\right]\{\Delta\tilde{d}\} = [\tilde{M}][\Delta t\{\dot{\tilde{d}}_i\} + \frac{1}{4}\Delta t^2\{\ddot{\tilde{d}}_i\}] + \frac{1}{4}\Delta t^2[\{\tilde{F}^{ext}_{i+1}\} - \{\tilde{F}^{int}_{i}\}] \tag{18}$$

The above equation is compacted by denoting the coefficient of $\{\Delta\tilde{d}\}$ as $[\tilde{K}^{eff}]$ and letting the right-hand side be $\{\tilde{F}^{eff}\}$; thus, we have

$$[\tilde{K}^{eff}]\{\Delta\tilde{d}\} = \{\tilde{F}^{eff}\} \tag{19}$$

At this point it is worthwhile to note that the implicit transient program may also be used for static analysis. The matrix form of the static incremental equation of equilibrium is

$$[\tilde{K}]\{\tilde{\Delta d}\} = \{\tilde{F}^{ext}_{i+1}\} - \{\tilde{F}^{int}_{i}\} \tag{20}$$

where the subscript now refers to the load step. Thus, it is seen that for a static problem we define the following matrices

$$[\tilde{K}^{eff}] = [\tilde{K}] \tag{21}$$

$$\{\tilde{F}^{eff}\} = \{\tilde{F}^{ext}_{i+1}\} - \{\tilde{F}^{int}_{i}\}$$

and solve Eq. (22) for the displacement increments. Equilibrium is checked by the equations of motion with the accelerations set equal to zero.

The computational procedure for each time step is described here. To begin, Eq. 13 is solved to give an estimate of the displacement increments from time step i to time step i+1. A Cholesky decomposition algorithm is used. The estimate of the new displacements is obtained by adding the displacement increments to the total displacement at the i^{th} step, that is

$$\{\tilde{d}_{i+1}\} = \{\tilde{d}_{i}\} + \{\tilde{\Delta d}\} \tag{22}$$

By rearranging Eq. 16, the new accelerations are found to be

$$\{\ddot{\tilde{d}}_{i+1}\} = \frac{4}{\Delta t^2}\left[\{\tilde{\Delta d}\} - \Delta t\{\dot{\tilde{d}}_{i}\} - \frac{\Delta t^2}{4}\{\ddot{\tilde{d}}_{i}\}\right] \tag{23}$$

The new velocities are obtained from Equation 17. The translational displacements, velocities, and accelerations obtained above for the i+1 time step are measured in the fixed global coordinate system. The angular quantities for the i+1 time step, however, are measured in the body coordinate system at the i^{th} time step. It is necessary to transform them to the body coordinate system at

the i+1 time step in order to make an equilibrium check. The updating is accomplished as follows. First, the increments in the body vectors are determined by

$$\{\Delta\bar{b}\}_j = [\Delta\bar{\theta}]\{\bar{b}^i\}_j \tag{24}$$

where

$[\Delta\bar{\theta}]$ = infinitesmal rotational matrix relative to the body coordinate system at time step i

$\{\bar{b}^i\}_j$ = components of unit body vector $\underline{b}_j$ in the body coordinate system at time step i

$\{\Delta\bar{b}\}_j$ = increment in body vector $\underline{b}_j$ relative to body coordinate system at time step i.

Next, the body vectors $\underline{b}_j$ at time step i+1 are given by

$$\{\bar{b}^{i+1}\}_j = \{\bar{b}^i\}_j + \{\Delta\bar{b}\}_j \tag{25}$$

where the components $\{\bar{b}^{i+1}\}_j$ are still measured relative to the body coordinate system at time i. The global components of $\underline{b}_j$ at the i+1 time step are obtained from

$$\{b^{i+1}\}_j = [\bar{T}^i]\{\bar{b}^{i+1}\}_j \tag{26}$$

where

$[\bar{T}^i]$ = the body to global transformation matrix at the i^{th} time step.

The body-to-global transformation matrix at the i+1 time step is now formed from the body vectors $\underline{b}_j^{i+1}$ as follows:

$$[\bar{T}^{i+1}] = [\{b^{i+1}\}_1 \{b^{i+1}\}_2 \{b^{i+1}\}_3] \tag{27}$$

The numerical procedure used to obtain the unit body vectors $\underline{b}_j^{i+1}$ is described in Ref. (1).

Because of the approximations made in arriving at Eq. 19, the predicted displacement, velocity, and acceleration fields will not, in general, satisfy the dynamic equilibrium equations (i.e., Eqs. 1 and 2). The degree to which the equilibrium equations are not satisfied is determined by comparing the nodal error energy to the sum of the internal and kinetic energies. Equilibrium is said to be satisfied when the error energy (Ref. 5) is less than a predetermined fraction of the system energy, that is

$$E^{err} < \gamma (E^K + E^I) \tag{28}$$

where E^{err} is the error energy, E^K is the kinetic energy, E^I is the internal strain energy, and γ is an error criterion. The error energy is determined in the following way. First, the nodal error forces are computed as the difference between the right- and left-hand sides of Eq. 15 at the $i+1$ time step, that is

$$\{\tilde{F}^{err}\} = \{\tilde{F}^{ext}_{i+1}\} - \{\tilde{F}^{int}_{i+1}\} - [\tilde{M}]\{\ddot{\hat{d}}_{i+1}\} \tag{29}$$

Then the error energy is defined as

$$E^{err} = \{\Delta\tilde{d}\}^T\{\tilde{F}^{err}\} \tag{30}$$

If the error energy exceeds the criterion, Eq. 19 is resolved with $\frac{1}{4}\Delta t^2\{F^{err}\}$ added to $\{F^{eff}\}$. This procedure is repeated until Eq. 28 is satisfied.

C. Deformation Field

When both the strains and variations in rotation within an element are relatively small, the displacement field within each element can be decomposed, with negligible error, into two components: rigid body motion, u_i^{rig}, and deformation, u_i^{def}:

$$u_i = u_i^{rig} + u_i^{def} \tag{31}$$

The motion of the corotational coordinate system defines the rigid body mode, while the deformation displacements are obtained by subtracting the rigid body displacements from the total displacements. The deformation field u_i^{def} within each element is approximated by a continuous interpolation function u_i^{*def}

$$u_i^{def} \cong u_i^{*def} = \psi_N d^{(N)} \qquad \text{(sum on N)} \tag{32}$$

where ψ_N is the shape function and $d^{(N)}$ is a measure of the deformation mode of an element.

For the triangular plate element herein considered, the shape functions are chosen such that the in-plane displacements, $\hat{u}_x^{def}$ and $\hat{u}_y^{def}$ are linear and the transverse displacement, u_z^{def}, is cubic. The interpolation functions are expressed in matrix notation as

$$\hat{u}_x^{def} = \{\psi_x^m\}^T \{\delta\} \tag{33}$$

$$\hat{u}_y^{def} = \{\psi_y^m\}^T \{\delta\} \tag{34}$$

and

$$\hat{u}_z^{def} = \{\psi^f\}^T \{\hat{\theta}\} \tag{35}$$

where

$$\{\delta\}^T = \{\delta_{12}\delta_{23}\delta_{31}\} \tag{36}$$

and

$$\{\hat{\theta}\}^T = \{\hat{\theta}_{1x} \; \hat{\theta}_{1y} \; \hat{\theta}_{2x} \; \hat{\theta}_{2y} \; \hat{\theta}_{3x} \; \hat{\theta}_{3y}\} \tag{37}$$

Here the discrete measures of element deformation are the element side elongations, δ_{IJ}, and the nodal rotations, $\hat{\theta}_{Ii}$, relative to the corotational coordinate system. The membrane shape functions, $\{\psi_x^m\}$ $\{\psi_y^m\}$, as well as the flexural shape function, $\{\psi^f\}$, are described in Appendix B.

D. Strain-Displacement Equations

As shown in Ref. 1, the engineering strains in each element are related to the local deformations by

$$\{\hat{\varepsilon}\} = [E^m]\{\delta\} - \hat{z}[E^f]\{\hat{\theta}\} \tag{38}$$

where

$$\{\hat{\varepsilon}\}^T = \{\hat{\varepsilon}_{xx}\ \hat{\varepsilon}_{yy}\ 2\hat{\varepsilon}_{xy}\} \tag{39}$$

The membrane strain-displacement matrix, $[E^m]$, and the flexural strain-displacement matrix, $[E^f]$, are described in Appendix B.

E. Internal Nodal Loads

The side forces, $\{f\}$, and the local moments, $\{\hat{m}\}$, constitute the local internal force matrix, $\{\hat{f}^{int}\}$, that is

$$\{\hat{f}^{int}\}^T = \{f_{12}\ f_{23}\ f_{31}\ \hat{m}_{1x}\ \hat{m}_{1y}\ \hat{m}_{2x}\ \hat{m}_{2y}\ \hat{m}_{3x}\ \hat{m}_{3y}\} \tag{40}$$

The side forces in each element, e, are defined as

$$\{f\} = \int_{V_e} [E^m]^T \{\hat{\sigma}\}\ dV_e \tag{41}$$

where

$$\{f\}^T = \{f_{12}\ f_{23}\ f_{31}\} \tag{42}$$

$$\{\hat{\sigma}\}^T = \{\hat{\sigma}_{xx}\ \hat{\sigma}_{yy}\ \hat{\sigma}_{xy}\} \tag{43}$$

while the local internal moments are defined as

$$\{\hat{m}\} = -\int_{V_e} \hat{z}[E^f]^T \{\hat{\sigma}\} dV_e \tag{44}$$

where

$$\{m\}^T = \{\hat{m}_{1x} \; \hat{m}_{1y} \; \hat{m}_{2x} \; \hat{m}_{2y} \; \hat{m}_{3x} \; \hat{m}_{3y}\} \tag{45}$$

V_e is the volume of element e.

The local internal forces, $\{\hat{f}^{int}\}$, are transformed to global coordinates by

$$\{f^{int}\} = [T]\{\hat{f}^{int}\} \tag{46}$$

where

$$\{f^{int}\}^T = \{f_{1x} \; f_{1y} \; f_{1z} \; m_{1x} \; m_{1y} \; m_{1z} \; f_{2x} \; f_{2y} \; f_{2z} \; m_{2x} \; m_{2y} \; m_{2z} \; f_{3x} \; f_{3y} \; f_{3z}\}$$

and the transformation matrix [T], is derived in Appendix A. The global internal forces are transformed to the mixed global-body coordinate system by

$$\{\tilde{f}^{int}\} = [\tilde{T}]\{f^{int}\} \tag{47}$$

where

$$\{\tilde{f}^{int}\}^T = \{f_{1x} \; f_{1y} \; f_{1z} \; \bar{m}_{1x} \; \bar{m}_{1y} \; \bar{m}_{1z} \; f_{2x} \; f_{2y} \; f_{2z} \; m_{2x} \; m_{2y} \; m_{2z}$$

$$f_{3x} \; f_{3y} \; f_{3z} \; \bar{m}_{3x} \; \bar{m}_{3y} \; \bar{m}_{3z}\}$$

and the transformation matrix, $[\tilde{T}]$, is also derived in Appendix A. The latter transformation is necessary because the rotational equations of motion are expressed in body coordinates.

F. Constitutive Equations

The material property coefficient matrix, $[\hat{C}]$ relates the element stresses to the engineering strains as follows:

$$\{\hat{\sigma}\} = [\hat{C}]\{\hat{\varepsilon}\} \tag{48}$$

where $[\hat{C}]$ may be a function of the stress, strain, or strain rate. The constitutive equation is assumed to relate the corotational stress and strain increments, that is

$$\{\Delta\hat{\sigma}\} = [\hat{C}_T]\{\Delta\hat{\varepsilon}\} \tag{49}$$

Since both $\{\Delta\hat{\sigma}\}$ and $\{\Delta\hat{\varepsilon}\}$ are frame indifferent, these relations satisfy the requirements of frame indifference. $[\hat{C}_T]$ is defined to be the tangential material property coefficient matrix. For an isotropic linear elastic material in a two-dimensional state of stress, the coefficient matrix is given by

$$[\hat{C}] = [\hat{C}_T] = \frac{E}{1-\nu^2}\begin{bmatrix} 1 & \nu & 0 \\ \nu & 1 & 0 \\ 0 & 0 & \frac{1-\nu}{2} \end{bmatrix} \tag{50}$$

where

E = Young's modulus

ν = Poisson's ratio .

For an elastic-plastic material, a linear relationship is developed between infinitesmals of stress and strain. Using the Prandtl-Reuss stress-strain relations along with the Von Mises yield criteria, the incremental relation in matrix form is given by (Ref. 6).

$$\{\Delta\hat{\sigma}\} = [\hat{C}_T(\hat{\sigma})]\{\Delta\hat{\varepsilon}\} \tag{51}$$

where $[\hat{C}_T]$ is the elastic-plastic material property coefficient matrix. For problems characterized by a two-dimensional state of stress, it is shown in Ref. 6 that

$$[\hat{C}_T] = \frac{1}{Q}\left[\begin{array}{cc|c} \hat{s}_y^2 + 2P & & s_y m. \\ -\hat{s}_x\hat{s}_y + 2\nu P & \hat{s}_x^2 + 2P & \\ \hline -\frac{\hat{s}_x+\nu\hat{s}_y}{1+\nu}\hat{s}_{xy} & -\frac{s_y+\nu s_x}{1+\nu}\hat{s}_{xy} & \frac{R}{2(1+\nu)} + \frac{2H'}{9E}(1-\nu)\bar{\sigma}^{-2} \end{array}\right] \tag{52}$$

where

s_x, s_y, s_{xy} = the deviatoric stress components

e, ν = Young's modulus and Poisson's ratio, respectively

$\bar{\sigma}$ = the equivalent stress

H' = the slope of the equivalent stress plastic strain curve

$P = \frac{2H'}{9E}\bar{\sigma}^{-2} + \frac{\hat{\sigma}_{xy}}{1+\nu}$

$R = \hat{s}_{xx}^2 + 2\nu\,\hat{s}_{xx}\hat{s}_{yy} + \hat{s}_{yy}^2$

$Q = R + 2(1-\nu^2)P$

G. Stiffness Matrices

The tangential and geometric stiffness matrices are developed in this section. From Eqs. 41 and 44, it is seen that the increments in element side forces and internal moments due to stress increments are given by

$$\{\Delta f\} = \int_{V_e} [E^m]^T \{\Delta\hat{\sigma}\}\, dV_e \tag{53}$$

and

$$\{\hat{m}\} = -\int_{V_e} \hat{z}\,[E^f]^T \{\Delta\hat{\sigma}\}\, dV_e \tag{54}$$

Using Eq. 48 to express the stress increments in terms of the strain increments and then expressing the strain increments in terms of the displacement increments via Eq. 38, the increments in internal forces are given by

$$\{\Delta\hat{f}^{int}\} = [\hat{k}_T]\,\{\Delta\hat{d}\} \tag{55}$$

where the element's local tangential stiffness, $[k_T]$, is defined as

$$[\hat{k}_T] = \int_{V_e} \begin{bmatrix} [E^m]^T [\hat{C}_T][E^m] & -\hat{z}[E^m]^T [\hat{C}_T][E^f] \\ -\hat{z}[E^f]^T [\hat{C}_T][E^m] & \hat{z}^2 [E^f]^T [C_T][E^f] \end{bmatrix} dV_e \tag{56}$$

Using the local-to-global transformation, $[T]$, the local element stiffness is transformed to the global coordinate system. Hence

$$[k_T] = [T][\hat{k}_T][T]^T \tag{57}$$

Now using the global-to-mixed coordinates transformation, $[\tilde{T}]$, the element stiffness is transformed by

$$[\tilde{k}_T] = [\tilde{T}][k_T][\tilde{T}]^T \tag{58}$$

The overall structural tangential stiffness matrix, $[\tilde{K}_T]$, in the mixed coordinate system is given by

$$[\tilde{K}_T] = \sum_{n=1}^{N} [L_T]^T_{(n)} [\tilde{k}_T]_{(n)} [L_T]_{(n)} \tag{59}$$

In order to handle problems with nonlinear geometric behavior, it is necessary to account for the change of geometry on the global equilibrium equation. This is accomplished by adding a geometric stiffness matrix to the tangential stiffness matrix. The membrane geometric stiffness matrix for a triangular plate element is developed in this section.

Martin (Ref. 7) has argued that it is primarily the axial load at the beginning of the increment that must be accounted for in large displacement problems. Initial bending moments are of secondary importance. Hence, for the triangular plate elements used in this code, only the membrane loads at the beginning of the increment are taken into account in the geometric stiffness matrix.

Recall that the increment in global nodal forces due to changes in geometry is given by

$$\{\Delta f^{int}\} = [\Delta T]^T_{ff} \{f^i\} \tag{60}$$

The transformation matrix, $[T]_{ff}$, is a function of the translational displacements, u_i, that is

$$[T]_{ff} = [T(u_{Ij})]_{ff} \tag{61}$$

where

u_{Ij} = the displacement of node I in the j^{th} direction. If we let $\{T\}_i$ denote the i^{th} column of $[T]^T_{ff}$ then

$$d\{T\}_i = \frac{\partial \{T\}_i}{\partial \{u\}} d\{u\} = \frac{\partial \{T\}_i}{\partial u_{1x}} \cdots \frac{\partial \{T\}_i}{\partial u_{3z}} d\{u\} \tag{62}$$

For small increments we have

$$\{\Delta T\}_i = [G]_i\{\Delta u\} \tag{63}$$

and

$$[G]_i = \left[\frac{\partial\{T\}_i}{\partial u_{1x}} \quad \cdots \frac{\partial\{T\}_i}{\partial u_{3z}} \right] \tag{64}$$

The $[G]_i$ matrices for the triangular plate element are evaluated in Appendix C.

The increment in the transformation matrix is now given by

$$[\Delta T]^T_{ff} = [G]_1\{\Delta u\} \ \ldots \ [G]_3\{\Delta u\} \tag{65}$$

Using Eq. 65, the second term on the right-hand side of Eq. 60 becomes

$$[\Delta T]^T_{ff}\{f^i\} = [G]_1\{\Delta u\}f^i_1 + [G]_2\{\Delta u\}f^i_2 + [G]_3\{\Delta u\}f^i_3 \tag{66}$$

which is seen to be equal to

$$[\Delta T]^T_{ff}\{f^i\} = \sum_{J=1}^{3} f^i_J [G]_J \{\Delta u\} \tag{67}$$

Defining the element's membrane geometric stiffness, $[k_G]$, at time step i as

$$[k_G] = \sum_{J=1}^{3} f^i_J [G]_J \tag{68}$$

and the second term of Eq. 60 becomes

$$[\Delta T^T_{ff}\{f^i\} = [k_G]\{\Delta u\} \tag{69}$$

The total structural geometric stiffness matrix, $[\tilde{K}_G]$, in the mixed coordinate system is given by

$$[\tilde{K}_G] = \sum_{n=1}^{N} [L_G]^T_{(n)} [k_G]_{(n)} [L_G]_{(n)} \tag{70}$$

It should be reemphasized that the geometric stiffness matrix as developed only pertains to the membrane loads. Hence, the terms in $[\tilde{K}_G]$ relative to the rotational degrees of freedom are zero.

The total structural stiffness matrix, $[\tilde{K}]$, is equal to the sum of the tangential stiffness matrix and the geometric stiffness matrix, that is

$$[\tilde{K}] = [\tilde{K}_T] + [\tilde{K}_G] \quad . \tag{71}$$

III. SAMPLE RESULTS

The code predicted response of several structural engineering problems are presented in this section and compared to either analytical or experimental results. The problems are chosen so that the various aspects of the code are checked.

A. Large Deflection of a Cantilever Plate

The first example deals with the elastic response of a cantilever plate subjected to an end load of sufficient magnitude to cause large displacements. This problem assesses the code's ability to treat structural problems with arbitrarily large rotations. The code results are compared to the analytical solution obtained by Bisshopp and Drucker (Ref. 8). The finite-element mesh along with comparative results are shown in Fig. 3. Good agreement for both the horizontal and vertical displacements is achieved.

B. Nonlinear Behavior of a Simply-Supported Plate and a Clamped Plate

The second problem considered is the nonlinear elastic response of a square plate subjected to a uniform lateral pressure. Two sets of boundary conditions are prescribed: simply supported and clamped all around. Unlike the previous problem in which the nonlinear behavior is due to large changes in geometry, the nonlinearity here is due to the large membrane forces generated by the stretching of the middle surface.

Figure 4 compares the central deflections obtained from the code to the analytical solutions (Refs. 9 and 10) for a square plate under constant lateral load. The code predicted deflections agree very closely with the analytical for both types of boundary conditions.

C. Dynamic Elastic Response of a Cantilever Beam

The third problem considered is the dynamic response of an end-loaded cantilever beam. The code results for displacement and velocity are compared to a three-

term model solution and to the explicit and implicit solutions of STRAW (Ref. 11). The finite-element model used for STRAW consists of six beam-type elements, while the three-dimensional code uses twelve plate-type elements. The meshes for both codes are shown in Fig. 5. A comparison of the tip displacement and tip velocity as a function of time for the various models is shown in Figs. 6 and 7, respectively. The results for the finite element models are seen to agree reasonably well with the modal solution.

D. Response of a Hexcan to Internal Pressure Pulses

The problem considered here is that of a duct subjected to a triangular pressure pulse. This problem was first studied by Kennedy (Ref. 13), using the explicit version of the STRAW code and subsequently by Schoeberle (Ref. 11), using the implicit version of STRAW. An axially-symmetric, internal triangular pressure pulse is assumed to load the hexcan (Fig. 8). Because of geometric and loading symmetries, a one-quarter strip model (Fig. 9) is used to represent the duct. The finite-element model consists of 24 triangular elements and 14 nodes.

The material properties of the hexcan are identical to those used in the previously-mentioned studies. Young's modulus is taken as $E = 23.5 \times 10^6$ psi, a yield stress of $\sigma_o = 57{,}000$ psi, a tangent modulus of $E_T = 3.45 \times 10^6$ psi, and a density of 7.35×10^{-4} lb-sec^2/in.^{4}.

The first study compares the results previously obtained from the STRAW code to those obtained with the three-dimensional implicit code. Two finite-element models were used with the STRAW code. The first model, a fine mesh representation, was a one-quarter symmetric-segment model which consists of 24 plane-strain beam elements (Fig. 10), and the second model, a coarse mesh representation, consisted of six plane-strain beam elements (Fig. 11). It should be noted that the 3-D model would correspond to the coarse STRAW model, since the side of each triangular element is the same length as the beam element. The applied load was the short-duration pressure pulse (Fig. 12A). The normal displacement history of the flat midpoint and the strain history on the outer surface at the flat midpoint, as predicted by STRAW, are shown in Figs. 13 and 14; while the results from the 3-D implicit code are shown in Figs. 15 and 16. The results are seen to agree fairly well. Figures 17 and 18 show the STRAW results for the normal displacement history of the corner and the strain history of the corner on the inside surface, respectively; Figs. 19 and 20 present the results obtained from the 3-D implicit code. A comparison of the above corner behavior indicates that there are significant differences between the

results predicted by the fine STRAW mesh and those of the coarse meshes (STRAW and 3-D implicit). This is to be expected, since the corner undergoes considerable localized plastic behavior which is better represented by the fine mesh. This comparison lucidly illustrates the importance of modeling technique in obtaining accurate results.

A study using the long-duration pressure pulse (Fig. 12B) was also conducted. The resulting normal displacement history of the flat's midpoint is shown in Figs. 21 and 22. The lack of oscillatory motion in the 3-D results is due to the larger time-step used: 50 μsec with the 3-D code vs 10 μsec with the STRAW code.

The third study compares the results obtained from SADCAT (an explicit code) to those obtained with the 3-D implicit code. The same finite-element model (Fig. 9) is used for both codes. The applied load is the long-duration pressure pulse (Fig. 12B). A 1 μsec time-step was used with SADCAT, and a 50 μsec time-step was used with the implicit 3-D code. Figures 22 and 23 show the normal displacement history of the flat midpoint. Here again, the agreement between the results is acceptable. As stated previously, the lack of oscillatory motion in the implicit results is due to the larger time-step used.

The above-studies were performed primarily to compare the results between the three codes: STRAW, SADCAT, and the 3-D implicit. By doing this, the newly-developed 3-D implicit code can be validated.

IV. SUMMARY

A finite-element procedure is formulated for the purpose of evaluating the integrity of thin structural components found in LMFBRs. The method is based upon the stiffness approach of structural mechanics and uses a diagonal mass matrix. The discretized equations of motion are integrated in time by an implicit integration algorithm. The code produces a step-by-step evolutive analysis for either long-duration dynamic, or static problems. The code can handle problems involving both nonlinear material and nonlinear geometric behavior. Presently the code is restricted as follows:

1. the structure must be thin (i.e., plate or shell types)
2. the external loading must be mechanical
3. although large displacements can be treated, the strains must be small.

Future developments with the code will eliminate the above limitations.

Several representative problems have been solved with the code for validative purposes. Comparison of code results with existing solutions shows good agreement.

APPENDIX A

TRANSFORMATION MATRICES

1. Coordinate Transformation Matrices

Vector components are transformed from one coordinate system to another by applying the appropriate coordinate transformation. The relation between body components and global components of an arbitrary vector, $\underline{v}$, is given by (Ref. 1)

$$\begin{Bmatrix} v_x \\ v_y \\ v_z \end{Bmatrix} = \begin{bmatrix} b_{1x} & b_{2x} & b_{3x} \\ b_{1y} & b_{2y} & b_{3y} \\ b_{1z} & b_{2z} & b_{3z} \end{bmatrix} \begin{Bmatrix} \bar{v}_x \\ \bar{v}_y \\ \bar{v}_z \end{Bmatrix} \tag{A1}$$

where b_{Ij} is the j-th component of the I-th unit body vector as shown in Fig. 1. Similarly, the relation between the corotational components of a vector, $\underline{v}$, and the global components of that vector is given by

$$\begin{Bmatrix} v_x \\ v_y \\ v_z \end{Bmatrix} = \begin{bmatrix} e_{1x} & e_{2x} & e_{3x} \\ e_{1y} & e_{2y} & e_{3y} \\ e_{1z} & e_{2z} & e_{3z} \end{bmatrix} \begin{Bmatrix} \hat{v}_x \\ \hat{v}_y \\ \hat{v}_z \end{Bmatrix} \tag{A2}$$

where e_{Ij} is the j-th component of the I-th unit corotational vector (Fig. 1).

2. Local Internal Force to Global Internal Force Transformation Matrix

The transformation matrix which relates the local internal force matrix, $\{\hat{f}^{int}\}$, to the global internal force matrix, $\{f^{int}\}$, is developed in this section. In Ref. 1 the relationships between the global nodal loads and the elements side forces and moments are given by

$$\begin{Bmatrix} f_{Ix} \\ f_{Iy} \\ f_{IZ} \end{Bmatrix} = \frac{f_{IJ}}{\ell_{IJ}} \begin{Bmatrix} x_{IJ} + u_{IJx} \\ y_{IJ} + u_{IJy} \\ z_{IJ} + u_{IJz} \end{Bmatrix} + \frac{f_{IK}}{\ell_{IK}} \begin{Bmatrix} x_{IK} + u_{IKx} \\ y_{IK} + u_{IKy} \\ z_{IK} + u_{IKz} \end{Bmatrix} + f_{Iz} \begin{Bmatrix} e_{3x} \\ e_{3y} \\ e_{3z} \end{Bmatrix} \tag{A3}$$

and

$$\begin{Bmatrix} \hat{f}_{1z} \\ \hat{f}_{2z} \\ \hat{f}_{3z} \end{Bmatrix} = \frac{1}{2A} \begin{bmatrix} \hat{x}_{23} & \hat{y}_{23} \\ \hat{x}_3 & \hat{y}_3 \\ -\hat{x}_2 & -\hat{y}_2 \end{bmatrix} \begin{Bmatrix} \hat{m}_{1x} + \hat{m}_{2x} + \hat{m}_{3x} \\ \hat{m}_{1y} + \hat{m}_{2y} + \hat{m}_{3y} \end{Bmatrix} \tag{A4}$$

where

$x_{IJ} = x_I - x_J$, $u_{IJx} = u_{Ix} - u_{Jx}$, etc

f_{IJ} = the force along side IJ of the element

ℓ_{IJ} = the current length of side IJ

A = the element area

The local moments at a generic node I are transformed to the global system by the transformation defined by Eq. A2, that is

$$\{m_I\} = [\hat{T}]\{\hat{m}_I\} \tag{A5}$$

Combining Eqs. A3, A4, and A5 for the three nodes of an element into a single matrix equation we obtain

$$\{f^{int}\} = [T]\{\hat{f}^{int}\} \tag{A6}$$

where

$$\{f^{int}\}^T = \{f_{1x}\ f_{1y}\ f_{1z}\ f_{2x}\ f_{2y}\ f_{2z}\ f_{3x}\ f_{3y}\ f_{3z}$$

$$m_{1x}\ m_{1y}\ m_{1z}\ m_{2x}\ m_{2y}\ m_{2z}\ m_{3x}\ m_{3y}\ m_{3z}\} \tag{A7}$$

$$\{\hat{f}^{int}\}^T = \{f_{12}\ f_{23}\ f_{31}\ \hat{m}_{1x}\ \hat{m}_{1y}\ \hat{m}_{1z}\ \hat{m}_{2x}\ \hat{m}_{2y}\ \hat{m}_{2z}\ \hat{m}_{3x}\ \hat{m}_{3y}\ \hat{m}_{3z}\} \tag{A8}$$

and

$$[T] = \begin{bmatrix} [T]_{ff} & [T]_{fm} \\ [0] & [T]_{mm} \end{bmatrix} \tag{A9}$$

and the submatrices in A9 are

$[T]_{ff}$ = the transformation matrix relating the element side forces to the global nodal forces

$[T]_{fm}$ = the transformation matrix relating the nodal moments in the local coordinate system to the nodal moments in the global system

$[T]_{mm}$ = the transformation matrix relating the nodal moments in the local system to the nodal moments in the global system.

Using relations A3, A4, and A5 the submatrices are given as follows

$$[T]_{ff} =$$

$$\begin{bmatrix}
1/\ell_{12}(x_{12}+u_{12x}) & 0 & -1/\ell_{31}(x_{31}+u_{31x}) \\
1/\ell_{12}(y_{12}+u_{12y}) & 0 & -1/\ell_{31}(y_{31}+u_{31y} \\
1/\ell_{12}(z_{12}+u_{12z} & 0 & -1/\ell_{31}(z_{31}+u_{31z}) \\
-1/\ell_{12}(x_{12}+u_{12x}) & 1/\ell_{23}(x_{23}+u_{23x}, & 0 \\
-1/\ell_{12}(y_{12}+u_{12y}) & 1/\ell_{23}(y_{23}+u_{23y}) & 0 \\
-1/\ell_{12}(z_{12}+u_{12z}) & 1/\ell_{23}(z_{23}+u_{23z}) & 0 \\
0 & -1/\ell_{23}(x_{23}+u_{23x}) & 1/\ell_{31}(x_{31}+u_{31x}) \\
0 & -1/\ell_{23}(y_{23}+u_{23y}) & 1/\ell_{31}(y_{31}+u_{31y}) \\
0 & -1/\ell_{23}(z_{23}+u_{23z}) & 1/\ell_{31}(z_{31}+u_{31z})
\end{bmatrix} \qquad \text{(A10)}$$

$$[T]_{fm} =$$

$$\frac{1}{2A}\begin{pmatrix}
\hat{x}_{23}e_{3x} & \hat{y}_{23}e_{3x} & 0 & \hat{x}_{23}e_{3x} & \hat{y}_{23}e_{3x} & 0 & \hat{x}_{23}e_{3x} & \hat{y}_{23}e_{3x} & 0 \\
\hat{x}_{23}e_{3y} & \hat{y}_{23}e_{3y} & 0 & \hat{x}_{23}e_{3y} & \hat{y}_{23}e_{3y} & 0 & \hat{x}_{23}e_{3y} & \hat{y}_{23}e_{3y} & 0 \\
\hat{x}_{23}e_{3z} & \hat{y}_{23}e_{3z} & 0 & \hat{x}_{23}e_{3z} & \hat{y}_{23}e_{3z} & 0 & \hat{x}_{23}e_{3z} & \hat{y}_{23}e_{3z} & 0 \\
\hat{x}_{3}e_{3x} & \hat{y}_{3}e_{3x} & 0 & \hat{x}_{3}e_{3x} & \hat{y}_{3}e_{3x} & 0 & \hat{x}_{3}e_{3x} & \hat{y}_{3}e_{3x} & 0 \\
\hat{x}_{3}e_{3y} & \hat{y}_{3}e_{3y} & 0 & \hat{x}_{3}e_{3y} & \hat{y}_{3}e_{3y} & 0 & \hat{x}_{3}e_{3y} & \hat{y}_{3}e_{3y} & 0 \\
\hat{x}_{3}e_{3z} & \hat{y}_{3}e_{3z} & 0 & \hat{x}_{3}e_{3z} & \hat{y}_{3}e_{3z} & 0 & \hat{x}_{3}e_{3z} & \hat{y}_{3}e_{3z} & 0 \\
-\hat{x}_{2}e_{3x} & -\hat{y}_{2}e_{3x} & 0 & -\hat{x}_{2}e_{3x} & -\hat{y}_{2}e_{3x} & 0 & -\hat{x}_{2}e_{3x} & -\hat{y}_{2}e_{3x} & 0 \\
-\hat{x}_{2}e_{3y} & -\hat{y}_{2}e_{3y} & 0 & -\hat{x}_{2}e_{3y} & -\hat{y}_{2}e_{3y} & 0 & -\hat{x}_{2}e_{3y} & -\hat{y}_{2}e_{3y} & 0 \\
-\hat{x}_{2}e_{3z} & -\hat{y}_{2}e_{3z} & 0 & -\hat{x}_{2}e_{3z} & -\hat{y}_{2}e_{3z} & 0 & -\hat{x}_{2}e_{3z} & -\hat{y}_{2}e_{3z} & 0
\end{pmatrix} \qquad \text{(A11)}$$

$$[T]_{mm} =$$

$$\begin{pmatrix}
e_{1x} & e_{2x} & e_{3x} & 0 & 0 & 0 & 0 & 0 & 0 \\
e_{1y} & e_{2y} & e_{3y} & 0 & 0 & 0 & 0 & 0 & 0 \\
e_{1z} & e_{2z} & e_{3z} & 0 & 0 & 0 & 0 & 0 & 0 \\
0 & 0 & 0 & e_{1x} & e_{2x} & e_{3x} & 0 & 0 & 0 \\
0 & 0 & 0 & e_{1y} & e_{2y} & e_{3y} & 0 & 0 & 0 \\
0 & 0 & 0 & e_{1z} & e_{2z} & e_{3z} & 0 & 0 & 0 \\
0 & 0 & 0 & 0 & 0 & 0 & e_{1x} & e_{2x} & e_{3x} \\
0 & 0 & 0 & 0 & 0 & 0 & e_{1y} & e_{2y} & e_{3y} \\
0 & 0 & 0 & 0 & 0 & 0 & e_{1z} & e_{2z} & e_{3z}
\end{pmatrix} \qquad \text{(A12)}$$

3. Global Coordinates to Mixed Coordinates Transformation Matrix

Since the translational equations of motion are written in the global coordinate system and the Euler equations are written in the body coordinate system, it is necessary to transform the moments and the corresponding terms in the stiffness matrices into the body coordinate system. The following transformation matrix, designated as $[\tilde{T}]$, is developed for this purpose.

Using the coordinate transformation, $[\bar{T}]$, the global moments at a node are transformed to the body coordinate system at that node by

$$\{\bar{m}\}_i = [\bar{T}]_i^T \{m\}_i \tag{A13}$$

where the subscript i indicates the node number. Using equation A13 it is seen that the global nodal moments are transformed to the body coordinate system by

$$\{\tilde{m}\} = [T^*]\{m\} \tag{A14}$$

where

$$\{\tilde{m}\}^T = [\bar{m}_{1x}\ \bar{m}_{1y}\ \bar{m}_{1z}\ \bar{m}_{2x}\ \bar{m}_{2y}\ \bar{m}_{2z}\ \bar{m}_{3x}\ \bar{m}_{3y}\ \bar{m}_{3z}] \tag{A15}$$

$$\{m\}^T = [m_{1x}\ m_{1y}\ m_{1z}\ m_{2x}\ m_{2y}\ m_{2z}\ m_{3x}\ m_{3y}\ m_{3z}] \tag{A16}$$

and

$$[T^*] = \begin{bmatrix} [\bar{T}]_1^T & [0] & [0] \\ [0] & [\bar{T}]_2^T & [0] \\ [0] & [0] & [\bar{T}]_3^T \end{bmatrix} \tag{A17}$$

Forming the global to mixed coordinate system transformation, $[\tilde{T}]$, as

$$[\tilde{T}] = \begin{bmatrix} [I] & [0] \\ [0] & [T^*] \end{bmatrix} \tag{A18}$$

where [I] is the identity matrix, it is seen that the global internal force matrix is transformed to the mixed system by

$$\{\bar{f}^{int}\} = [\bar{T}]\{f^{int}\} \tag{A19}$$

APPENDIX B

SHAPE FUNCTIONS AND STRAIN-DISPLACEMENT MATRICES

1. Membrane Strain-Displacement Matrix

The strain-displacement matrix, $[E^m]$, which relates the engineering strains to the side elongations of the triangular plane element were formulated by Marchertas and Belytschko (Ref. 1). Their final results are

$$\{\hat{\varepsilon}\} = [E^m]\{\delta\} \tag{B1}$$

where

$$[E^m] = \begin{bmatrix} [(\ell_{z1}+\ell_{z1})/(4\ell_{z1}\ell^0_{z1})](\ell_{z1}/\hat{x}_{z1})^2 & -[\ell^2_{z2}/(4\ell_{z1}\ell_{z1}\ell^0_{z2})](\ell_{z1}/\hat{x}_{z1})^2 & [(\ell_{z1}+\ell_{z1})/(4\ell_{z1}\ell^0_{z1})](\ell_{z1}/\hat{x}_{z1})^2 \\ [(\ell_{z1}-\ell_{z1})/(4\ell_{z1}\ell^0_{z1})](\ell_{z1}/\hat{y}_{z1})^2 & [\ell^2_{z2}/(4\ell_{z1}\ell_{z1}\ell^0_{z2})](\ell_{z1}/\hat{y}_{z1})^2 & -[(\ell_{z1}-\ell_{z1})/(4\ell_{z1}\ell^0_{z1})](\ell_{z1}/\hat{y}_{z1})^2 \\ (\ell_{z1}/\hat{x}_{z1})(\ell_{z1}/\hat{y}_{z1})/(2\ell^0_{z1}) & 0 & -(\ell_{z1}/\hat{x}_{z1})(\ell_{z1}/\hat{y}_{z1})/(2\ell^0_{z1}) \end{bmatrix} \tag{B2}$$

2. Flexural Shape Functions and Strain-Displacement Matrix

Using the cubic deflection function given by Zienkiewicz (Ref.12) the following shape functions, ψ^f_i, are obtained by Marchertas and Belytschko (Ref. 1)

$$\left.\begin{aligned} \varphi^f_1 &= b_2(\zeta_1^2\zeta_3 + 0.5\zeta_1\zeta_2\zeta_3) - b_3(\zeta_1^2\zeta_2 + 0.5\zeta_1\zeta_2\zeta_3), \\ \varphi^f_2 &= a_2(\zeta_1^2\zeta_3 + 0.5\zeta_1\zeta_2\zeta_3) - a_3(\zeta_1^2\zeta_2 + 0.5\zeta_1\zeta_2\zeta_3), \\ \varphi^f_3 &= b_3(\zeta_2^2\zeta_1 + 0.5\zeta_1\zeta_2\zeta_3) - b_1(\zeta_2^2\zeta_3 + 0.5\zeta_1\zeta_2\zeta_3), \\ \varphi^f_4 &= a_3(\zeta_2^2\zeta_1 + 0.5\zeta_1\zeta_2\zeta_3) - a_1(\zeta_2^2\zeta_3 + 0.5\zeta_1\zeta_2\zeta_3), \\ \varphi^f_5 &= b_1(\zeta_3^2\zeta_2 + 0.5\zeta_1\zeta_2\zeta_3) - b_2(\zeta_3^2\zeta_1 + 0.5\zeta_1\zeta_2\zeta_3), \\ \varphi^f_6 &= a_1(\zeta_3^2\zeta_2 + 0.5\zeta_1\zeta_2\zeta_3) - a_2(\zeta_3^2\zeta_1 + 0.5\zeta_1\zeta_2\zeta_3), \end{aligned}\right\} \tag{B3}$$

where

ζ_1, ζ_2, and ζ_3 = triangular coordinates

a_i and b_i = lengths defined in Fig. 2

The flexural strain-displacement matrix is defined as

$$[E^f] = \begin{bmatrix} \partial^2\psi_I^f/\partial\hat{x}^2 \\ \partial^2\psi_I^f/\partial\hat{y}^2 \\ \partial^2\psi_I^f/\partial\hat{x}\partial\hat{y} \end{bmatrix} \tag{B4}$$

Since a numerical integration scheme is used in evaluating the integral containing $[E^f]$ in Eq. 56), it is necessary only to evaluate $[E^f]$ at the three integration points (points 4-6 shown in Fig. 2). As shown in Ref. 1 these expressions are

1. For point 4 ($\zeta_1 = 0,\ \zeta_2 = 0.5,\ \zeta_3 = 0.5$):

$$
\left.
\begin{aligned}
\partial^2\varphi_1^f/\partial\hat{x}^2 &= 0.5b_1(b_3^2 - b_2^2)/(2A)^2 \\
\partial^2\varphi_2^f/\partial\hat{x}^2 &= 0.5b_1^2(a_2 - a_3)/(2A)^2 \\
\partial^2\varphi_3^f/\partial\hat{x}^2 &= b_1[0.5b_2(3b_3 - b_2) + b_3^2]/(2A)^2 \\
\partial^2\varphi_4^f/\partial\hat{x}^2 &= [0.5b_1^2(a_1 - a_3) - b_2(a_1b_2 + 4A)]/(2A)^2 \\
\partial^2\varphi_5^f/\partial\hat{x}^2 &= b_1[0.5b_3(b_3 - 3b_2) - b_2^2]/(2A)^2 \\
\partial^2\varphi_6^f/\partial\hat{x}^2 &= [0.5b_1^2(a_2 - a_1) + b_3(a_1b_3 - 4A)]/(2A)^2 \\
\partial^2\varphi_1^f/\partial\hat{y}^2 &= 0.5a_1^2(b_2 - b_3)/(2A)^2 \\
\partial^2\varphi_2^f/\partial\hat{y}^2 &= 0.5a_1(a_3^2 - a_2^2)/(2A)^2 \\
\partial^2\varphi_3^f/\partial\hat{y}^2 &= [0.5a_1^2(b_1 - b_3) - a_2(a_2b_1 - 4A)]/(2A)^2 \\
\partial^2\varphi_4^f/\partial\hat{y}^2 &= a_1[0.5a_2(3a_3 - a_2) + a_3^2]/(2A)^2 \\
\partial^2\varphi_5^f/\partial\hat{y}^2 &= [0.5a_1^2(b_2 - b_1) + a_3(a_3b_1 + 4A)]/(2A)^2 \\
\partial^2\varphi_6^f/\partial\hat{y}^2 &= a_1[0.5a_3(a_3 - 3a_2) - a_2^2]/(2A)^2 \\
\partial^2\varphi_1^f/\partial\hat{x}\partial\hat{y} &= 0.5a_1b_1(b_2 - b_3)/(2A)^2 \\
\partial^2\varphi_2^f/\partial\hat{x}\partial\hat{y} &= 0.5a_1b_1(a_2 - a_3)/(2A)^2 \\
\partial^2\varphi_3^f/\partial\hat{x}\partial\hat{y} &= a_1(b_1^2 - b_2^2 + 0.5b_1b_2)/(2A)^2 \\
\partial^2\varphi_4^f/\partial\hat{x}\partial\hat{y} &= b_1(a_1^2 - a_2^2 + 0.5a_1a_2)/(2A)^2 \\
\partial^2\varphi_5^f/\partial\hat{x}\partial\hat{y} &= a_1(b_3^2 - b_1^2 - 0.5b_1b_3)/(2A)^2
\end{aligned}
\right\}. \qquad (B5)
$$

2. For point 5 ($\zeta_1 = 0.5$, $\zeta_2 = 0$, $\zeta_3 = 0.5$):

$$
\begin{aligned}
\partial^2\varphi_1^f/\partial\hat{x}^2 &= b_2[0.5b_1(b_1 - 3b_3) - b_3^2]/(2A)^2 \\
\partial^2\varphi_2^f/\partial\hat{x}^2 &= [0.5b_2^2(a_3 - a_2) + b_1(a_2b_1 - 4A)]/(2A)^2 \\
\partial^2\varphi_3^f/\partial\hat{x}^2 &= 0.5b_2(b_1^2 - b_3^2)/(2A)^2 \\
\partial^2\varphi_4^f/\partial\hat{x}^2 &= 0.5b_2^2(a_3 - a_1)/(2A)^2 \\
\partial^2\varphi_5^f/\partial\hat{x}^2 &= b_2[0.5b_3(3b_1 - b_3) + b_1^2]/(2A)^2 \\
\partial^2\varphi_6^f/\partial\hat{x}^2 &= [0.5b_2^2(a_2 - a_1) - b_3(a_2b_3 + 4A)]/(2A)^2 \\
\partial^2\varphi_1^f/\partial\hat{y}^2 &= [0.5a_2^2(b_3 - b_2) + a_1(a_1b_2 + 4A)]/(2A)^2 \\
\partial^2\varphi_2^f/\partial\hat{y}^2 &= a_2[0.5a_1(a_1 - 3a_3) - a_3^2]/(2A)^2 \\
\partial^2\varphi_3^f/\partial\hat{y}^2 &= 0.5a_2^2(b_3 - b_1)/(2A)^2 \\
\partial^2\varphi_4^f/\partial\hat{y}^2 &= 0.5a_2(a_1^2 - a_3^2)/(2A)^2 \\
\partial^2\varphi_5^f/\partial\hat{y}^2 &= [0.5a_2^2(b_2 - b_1) - a_3(a_3b_2 - 4A)]/(2A)^2 \\
\partial^2\varphi_6^f/\partial\hat{y}^2 &= a_2[0.5a_3(3a_1 - a_3) + a_1^2]/(2A)^2 \\
\partial^2\varphi_1^f/\partial\hat{x}\partial\hat{y} &= a_2(b_1^2 - b_2^2 - 0.5b_1b_2)/(2A)^2 \\
\partial^2\varphi_2^f/\partial\hat{x}\partial\hat{y} &= b_2(a_1^2 - a_2^2 - 0.5a_1a_2)/(2A)^2 \\
\partial^2\varphi_3^f/\partial\hat{x}\partial\hat{y} &= 0.5a_2b_2(b_3 - b_1)/(2A)^2 \\
\partial^2\varphi_4^f/\partial\hat{x}\partial\hat{y} &= 0.5a_2b_2(a_3 - a_1)/(2A)^2 \\
\partial^2\varphi_5^f/\partial\hat{x}\partial\hat{y} &= a_2(b_2^2 - b_3^2 + 0.5b_2b_3)/(2A)^2 \\
\partial^2\varphi_6^f/\partial\hat{x}\partial\hat{y} &= b_2(a_2^2 - a_3^2 + 0.5a_2a_3)/(2A)^2
\end{aligned}
\tag{B6}
$$

3. For point 6 ($\zeta_1 = 0.5$, $\zeta_2 = 0.5$, $\zeta_3 = 0$):

$$
\begin{aligned}
\partial^2\varphi_1^f/\partial\hat{x}^2 &= b_3[0.5b_1(3b_2 - b_1) + b_2^2]/(2A)^2 \\
\partial^2\varphi_2^f/\partial\hat{x}^2 &= [0.5b_3^2(a_3 - a_2) - b_1(a_3b_1 + 4A)]/(2A)^2 \\
\partial^2\varphi_3^f/\partial\hat{x}^2 &= b_3[0.5b_2(b_2 - 3b_1) - b_1^2]/(2A)^2 \\
\partial^2\varphi_4^f/\partial\hat{x}^2 &= [0.5b_3^2(a_1 - a_3) + b_2(a_3b_2 - 4A)]/(2A)^2 \\
\partial^2\varphi_5^f/\partial\hat{x}^2 &= 0.5b_3(b_2^2 - b_1^2)/(2A)^2 \\
\partial^2\varphi_6^f/\partial\hat{x}^2 &= 0.5b_3^2(a_1 - a_2)/(2A)^2 \\
\partial^2\varphi_1^f/\partial\hat{y}^2 &= [0.5a_3^2(b_3 - b_2) - a_1(a_1b_3 - 4A)]/(2A)^2 \\
\partial^2\varphi_2^f/\partial\hat{y}^2 &= a_3[0.5a_1(3a_2 - a_1) + a_2^2]/(2A)^2 \\
\partial^2\varphi_3^f/\partial\hat{y}^2 &= [0.5a_3^2(b_1 - b_3) + a_2(a_2b_3 + 4A)]/(2A)^2 \\
\partial^2\varphi_4^f/\partial\hat{y}^2 &= a_3[0.5a_2(a_2 - 3a_1) - a_1^2]/(2A)^2 \\
\partial^2\varphi_5^f/\partial\hat{y}^2 &= 0.5a_3^2(b_1 - b_2)/(2A)^2 \\
\partial^2\varphi_6^f/\partial\hat{y}^2 &= 0.5a_3(a_2^2 - a_1^2)/(2A)^2 \\
\partial^2\varphi_1^f/\partial\hat{x}\partial\hat{y} &= a_3(b_3^2 - b_1^2 + 0.5b_1b_3)/(2A)^2 \\
\partial^2\varphi_2^f/\partial\hat{x}\partial\hat{y} &= b_3(a_3^2 - a_1^2 + 0.5a_1a_3)/(2A)^2 \\
\partial^2\varphi_3^f/\partial\hat{x}\partial\hat{y} &= a_3(b_2^2 - b_3^2 - 0.5b_2b_3)/(2A)^2 \\
\partial^2\varphi_4^f/\partial\hat{x}\partial\hat{y} &= b_3(a_2^2 - a_3^2 - 0.5a_2a_3)/(2A)^2 \\
\partial^2\varphi_5^f/\partial\hat{x}\partial\hat{y} &= 0.5a_3b_3(b_1 - b_2)/(2A)^2 \\
\partial^2\varphi_6^f/\partial\hat{x}\partial\hat{y} &= 0.5a_3b_3(a_1 - a_2)/(2A)^2
\end{aligned}
\qquad \text{(B7)}
$$

APPENDIX C

EVALUATION OF $[G]_i$ MATRICES

The $[G]_i$ matrices as formulated in the text are defined as

$$[G]_i = \left[\frac{\partial\{T\}_i}{\partial u_{1x}} \cdots \frac{\partial\{T\}_i}{\partial u_{3z}}\right] \tag{C1}$$

where $\{T\}_i$ is the i-th column of the $[T]_{ff}^T$ matrix. Using the side force to global nodal force transformation matrix, $[T]_{ff}$ (as given in Appendix A), the following expressions are obtained for the [G] matrices.

$[G]_1$ =

$$\begin{pmatrix}
1/\ell_1 & 0 & 0 & -1/\ell_1 & 0 & 0 & 0 & 0 & 0 \\
0 & 1/\ell_1 & 0 & 0 & -1/\ell_1 & 0 & 0 & 0 & 0 \\
0 & 0 & 1/\ell_1 & 0 & 0 & -1/\ell_1 & 0 & 0 & 0 \\
0 & 0 & 0 & 0 & 0 & 0 & 0 & 0 & 0 \\
0 & 0 & 0 & 0 & 0 & 0 & 0 & 0 & 0 \\
0 & 0 & 0 & 0 & 0 & 0 & 0 & 0 & 0 \\
1/\ell_3 & 0 & 0 & 0 & 0 & 0 & -1/\ell_3 & 0 & 0 \\
0 & 1/\ell_3 & 0 & 0 & 0 & 0 & 0 & -1/\ell_3 & 0 \\
0 & 0 & 1/\ell_3 & 0 & 0 & 0 & 0 & 0 & -1/\ell_3
\end{pmatrix} \quad (C2)$$

$$[G]_2 =$$

$$\begin{pmatrix}
-1/\ell_1 & 0 & 0 & 1/\ell_1 & 0 & 0 & 0 & 0 & 0 \\
0 & -1/\ell_1 & 0 & 0 & 1/\ell_1 & 0 & 0 & 0 & 0 \\
0 & 0 & -1/\ell_1 & 0 & 0 & 1/\ell_1 & 0 & 0 & 0 \\
0 & 0 & 0 & 1/\ell_2 & 0 & 0 & -1/\ell_2 & 0 & 0 \\
0 & 0 & 0 & 0 & 1/\ell_2 & 0 & 0 & -1/\ell_2 & 0 \\
0 & 0 & 0 & 0 & 0 & 1/\ell_2 & 0 & 0 & -1/\ell_2 \\
0 & 0 & 0 & 0 & 0 & 0 & 0 & 0 & 0 \\
0 & 0 & 0 & 0 & 0 & 0 & 0 & 0 & 0 \\
0 & 0 & 0 & 0 & 0 & 0 & 0 & 0 & 0
\end{pmatrix} \quad (C$$

$[G]_3 =$

$$\begin{pmatrix}
0 & 0 & 0 & 0 & 0 & 0 & 0 & 0 & 0 \\
0 & 0 & 0 & 0 & 0 & 0 & 0 & 0 & 0 \\
0 & 0 & 0 & 0 & 0 & 0 & 0 & 0 & 0 \\
0 & 0 & 0 & -1/\ell_2 & 0 & 0 & 1/\ell_2 & 0 & 0 \\
0 & 0 & 0 & 0 & -1/\ell_2 & 0 & 0 & 1/\ell_2 & 0 \\
0 & 0 & 0 & 0 & 0 & -1/\ell_2 & 0 & 0 & 1/\ell_2 \\
-1/\ell_3 & 0 & 0 & 0 & 0 & 0 & 1/\ell_3 & 0 & 0 \\
0 & -1/\ell_3 & 0 & 0 & 0 & 0 & 0 & 1/\ell_3 & 0 \\
0 & 0 & -1/\ell_3 & 0 & 0 & 0 & 0 & 0 & 1/\ell_3
\end{pmatrix} \qquad (C4)$$

ACKNOWLEDGMENTS

The authors wish to thank the following people for their assistance: Dr. A. H. Marchertas, for his helpful explanations concerning the SADCAT code; Drs. S. H. Fistedis and J. M. Kennedy, for their direction and encouragement; and to Mr. C. Fiala, for his programming assistance.

REFERENCES

1. A. H. Marchertas and T. B. Belytschko, Nonlinear Finite-Element Formulation for Transient Analysis of Three-Dimensional Thin Structures, ANL-8104 (June 1974).

2. J. H. Argyris, S. Kelsey, and H. Kamel, "Matrix Methods of Structural Analysis: A Precis of Recent Developments," Matrix Methods of Structural Analysis, ed. B. F. deVeubeke, AGARDograph 72, Pergamon Press (1964).

3. T. J. Oden, Finite Elements of Nonlinear Continua, McGraw-Hill Book Co., Inc., New York (1972).

4. N. M. Newmark, A Method of Computation for Structural Dynamics, J. Eng. Mech., Div. of ASCE 85, 67-94 (1959).

5. T. Belytschko and D. F. Schoeberle, On the Unconditional Stability of an Implicit Algorithm for Nonlinear Structural Dynamics, to be published, J. Appl. Mech.

6. Y. Yamada, N. Yoshimura, and T. Sakurai, Plastic Stress-Strain Matrix and its Application for the Solution of Elastic-Plastic Problems by the Finite Element Method, Int. J. Mech. Sci., 10, 343-354 (1968).

7. H. C. Martin, "On the Derivation of Stiffness Matrices for the Analysis of Large Deflection and Stability Problems," Conference on Matrix Methods in Structural Mechanics, Wright Patterson Air Force Base (1965).

8. K. E. Bisshopp and D. C. Drucker, Large Deflection of Cantilever Beams, Quarterly of Applied Math., Vol. III, No. 3, pp. 272-275 (1945).

9. S. Levy, Bending of Rectangular Plates with Large Deflections, NACA Report 737, National Advisory Committee for Aeronautics, Washington, D. C., (1942).

10. S. Levy, Square Plates with Clamped Edges under Normal Pressure, NACA Report 740, National Advisory Committee for Aeronautics, Washington, D. C. (1942).

11. D. F. Schoeberle, J. M. Kennedy, and T. B. Belytschko, Implicit Temporal Integration for Long-Duration Accidents in a Structural Response Code--STRAW, ANL-8136 (Oct. 1974).

12. O. C. Zienkiewicz, The Finite Element Method in Engineering Science, McGraw-Hill Book Co., Inc., London (1972).

13. J. M. Kennedy, Nonlinear Dynamic Response of Reactor-Core Subassemblies, ANL-8065 (January 1974).

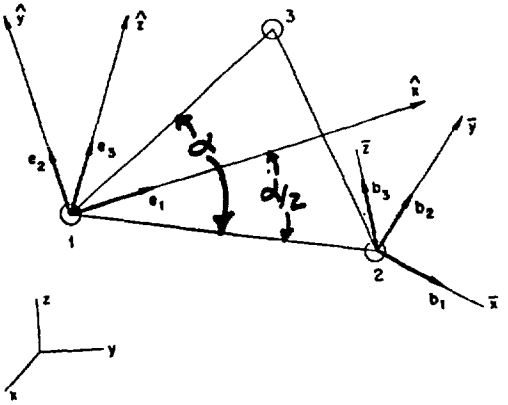

Fig. 1. Coordinate Systems.
ANL Neg. No. 900-3469.

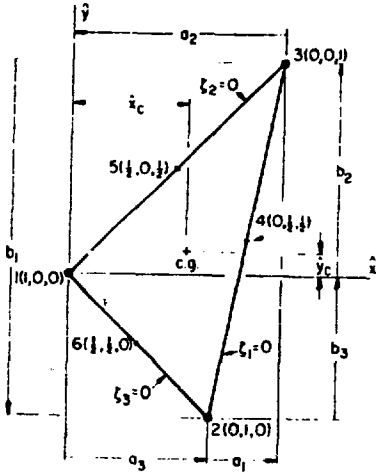

$a_1 = \hat{x}_3 - \hat{x}_2$ $\quad b_1 = \hat{y}_2 - \hat{y}_3$

$a_2 = -\hat{x}_3$ $\quad b_2 = \hat{y}_3$

$a_3 = \hat{x}_2$ $\quad b_3 = -\hat{y}_2$

$\hat{x}_c = (\hat{x}_2 + \hat{x}_3)/3 = (a_3 - a_2)/3$

$\hat{y}_c = (\hat{y}_2 + \hat{y}_3)/3 = (b_2 - b_3)/3$

Fig. 2 Definition of Element Coordinates

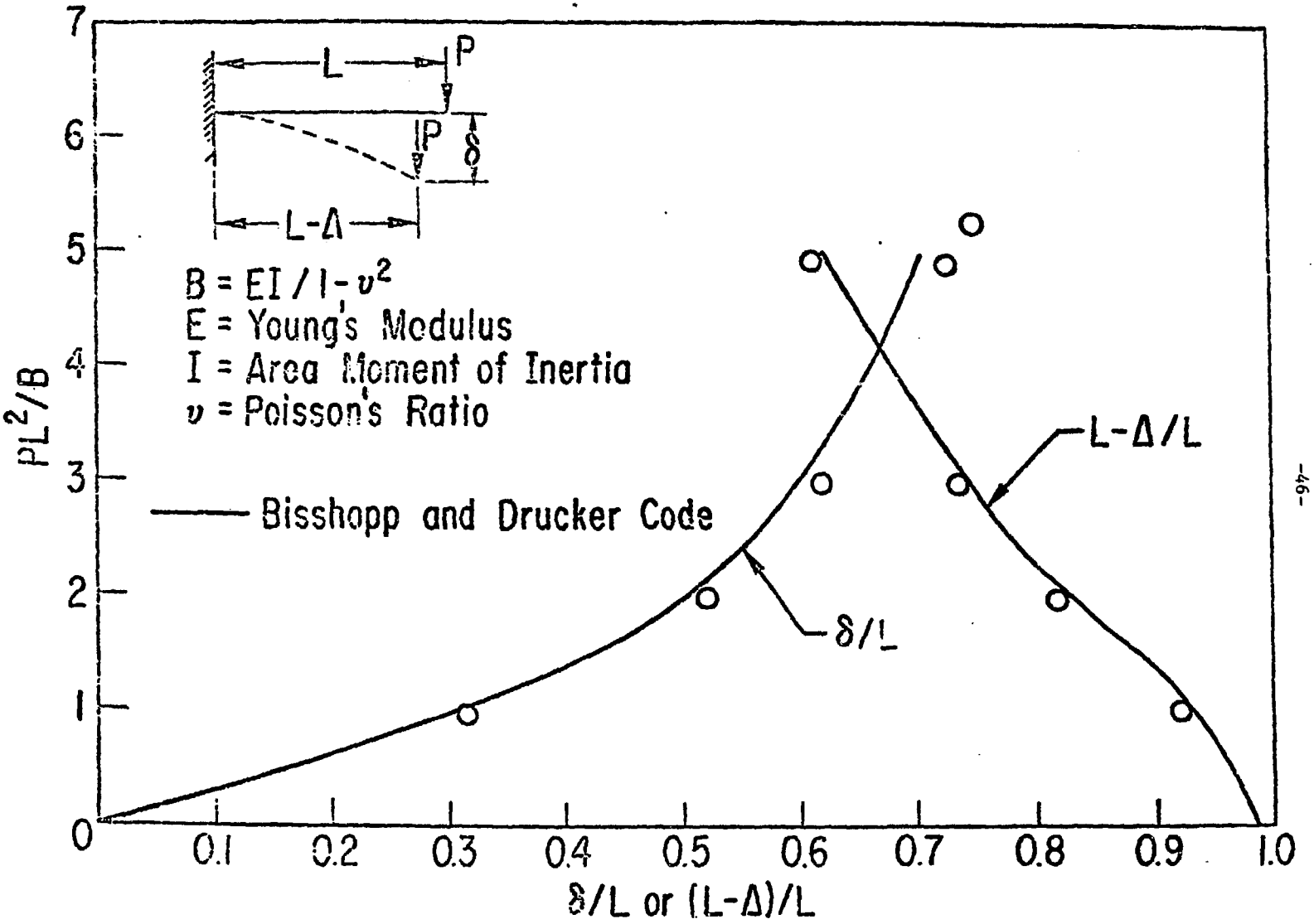

Fig. 3 Comparison Between Predicted Code Displacements and Analytical Results for the Large Displacement of a Cantilever Plate.

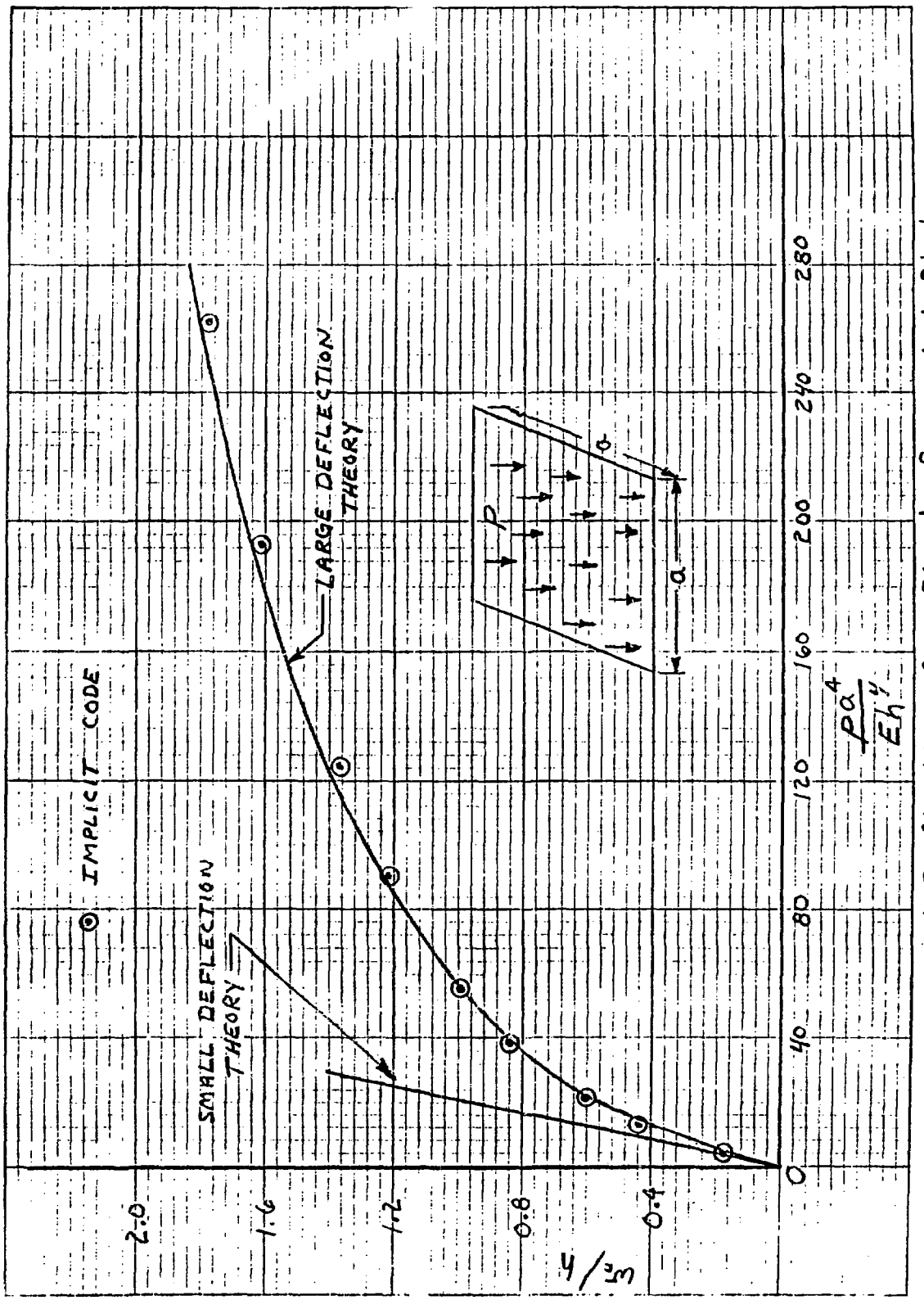

Fig. 4 Central Deflection of a Simply Supported Plate

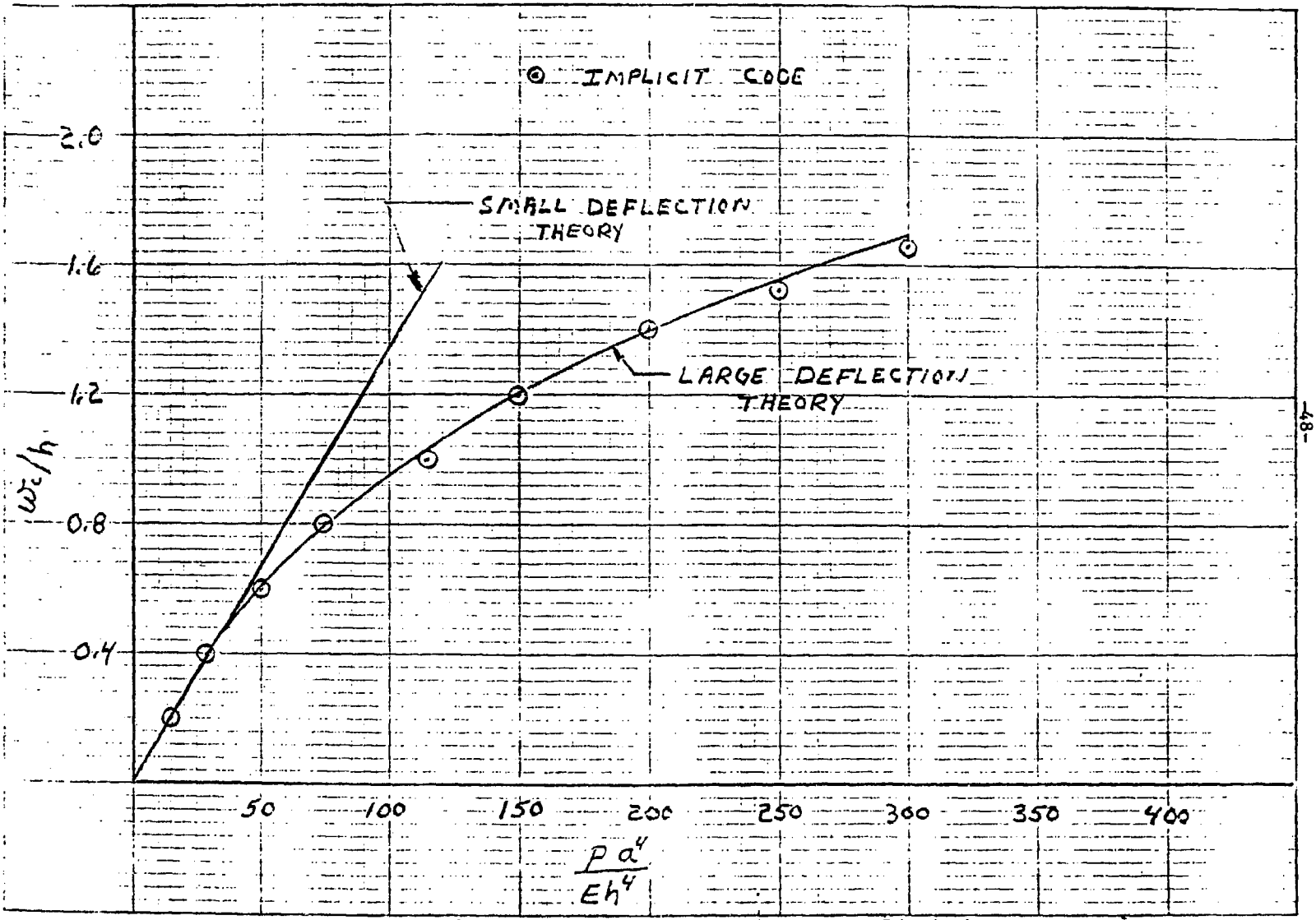

Fig. 5. Central Deflection of a Clamped Plate

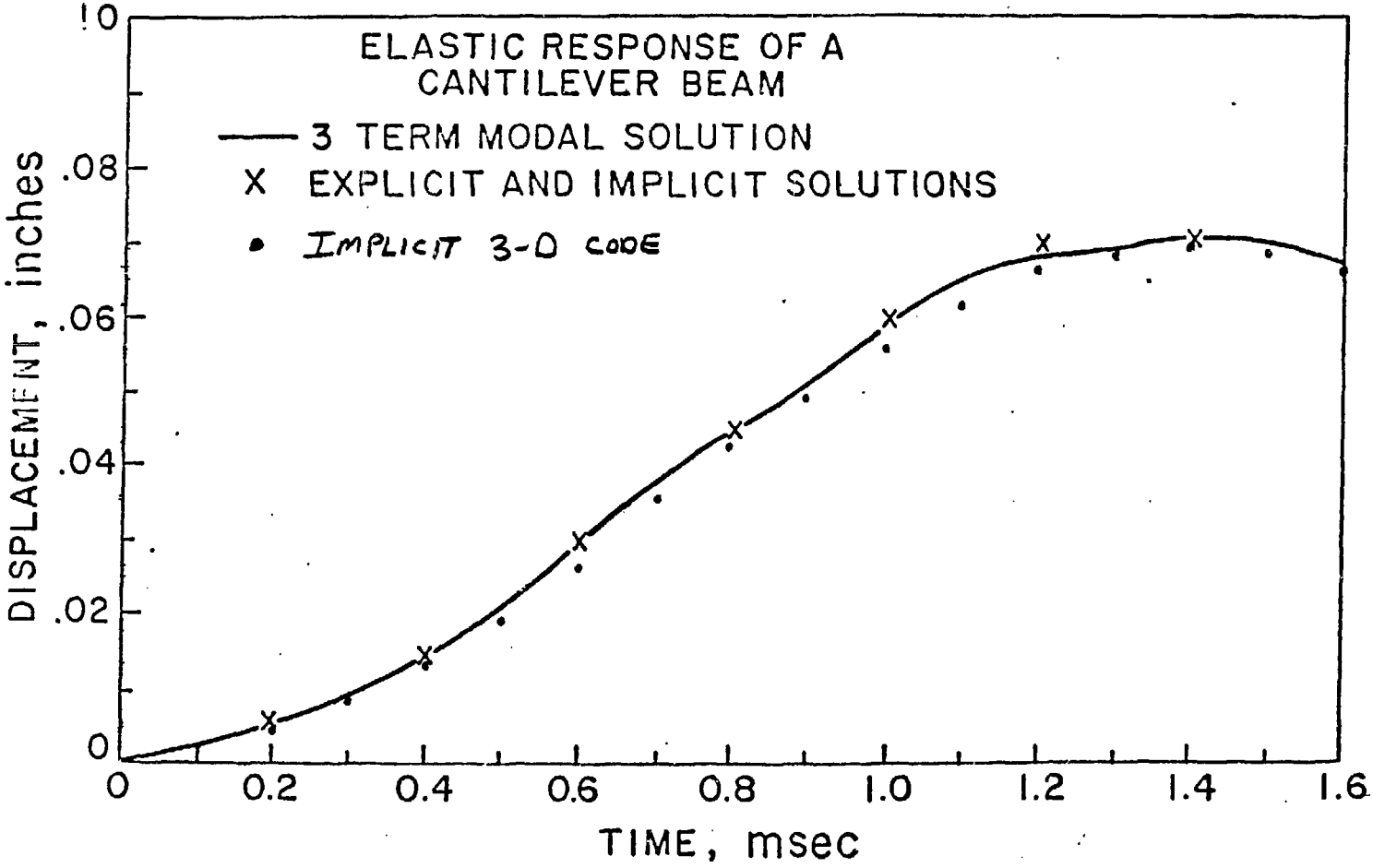

Figure 6. Displacement-Time History for an Elastic Cantilever Beam.

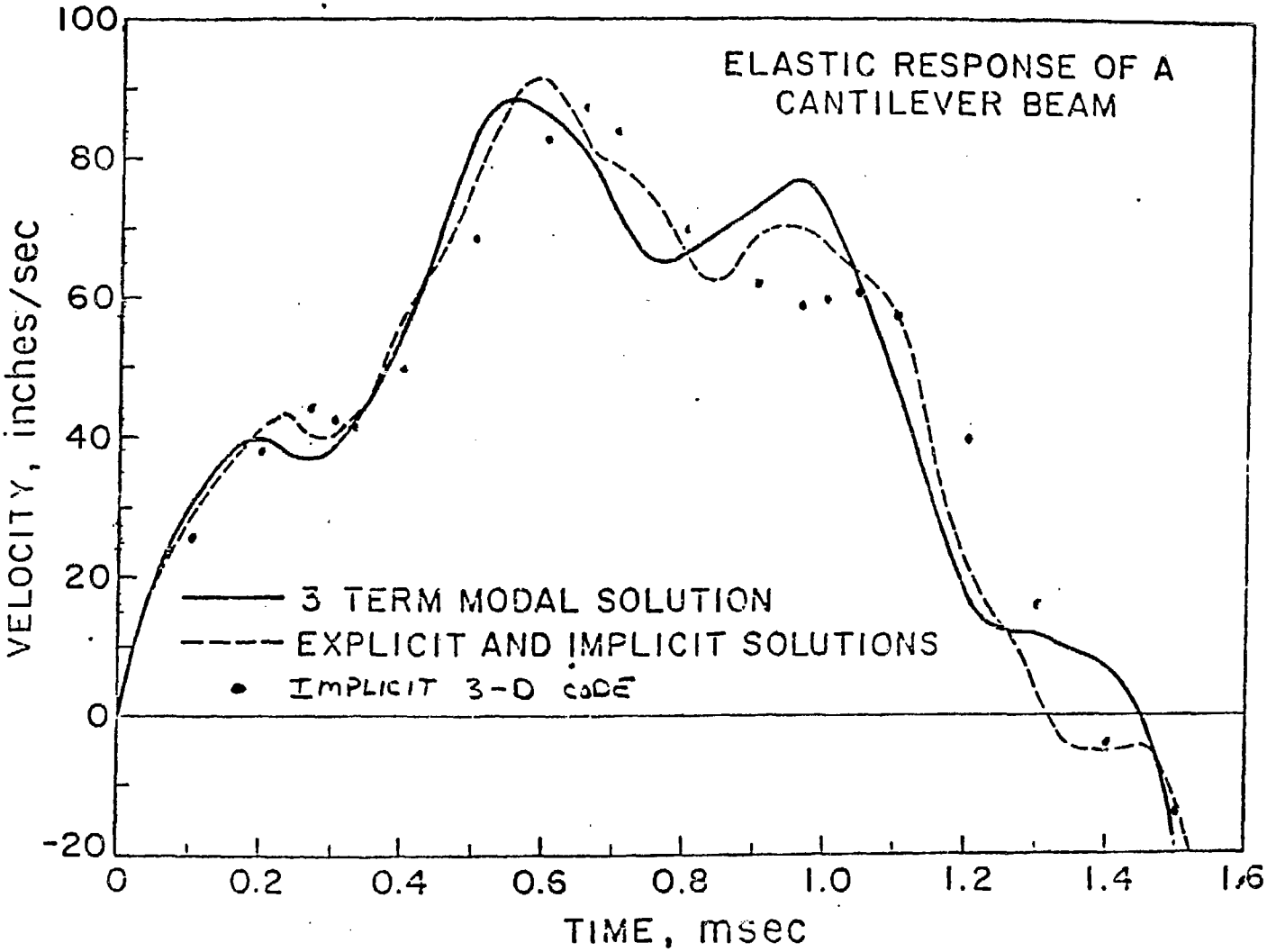

Figure 7. Velocity-Time History for an Elastic Cantilever Beam

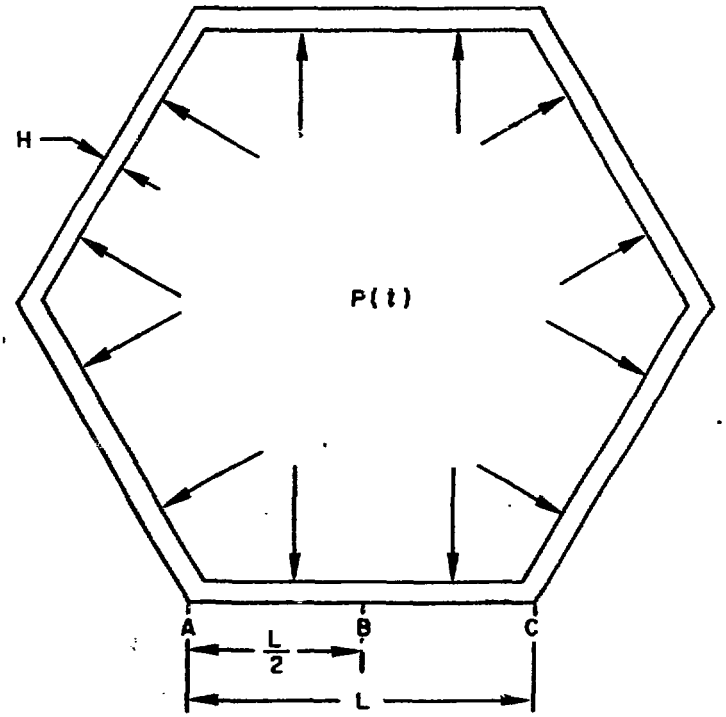

Fig. 8. Internally Pressurized Hexcan

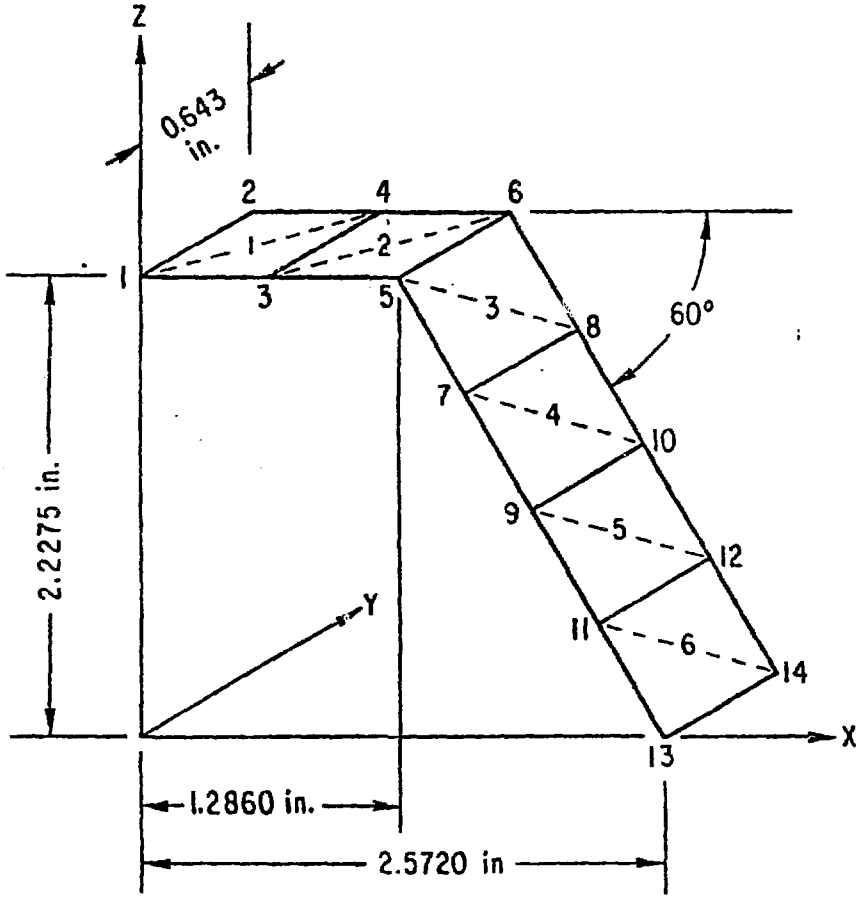

Fig. 9. Strip Model for One-fourth of a Hexcan.

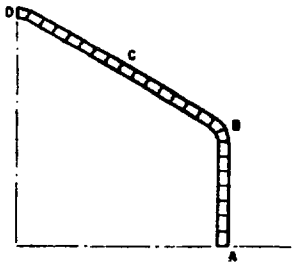

Fig. 10

One-quarter Finite-element Model (Fine mesh)

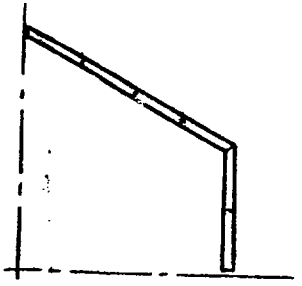

Fig. 11. One-quarter Finite-element Model (Coarse mesh)

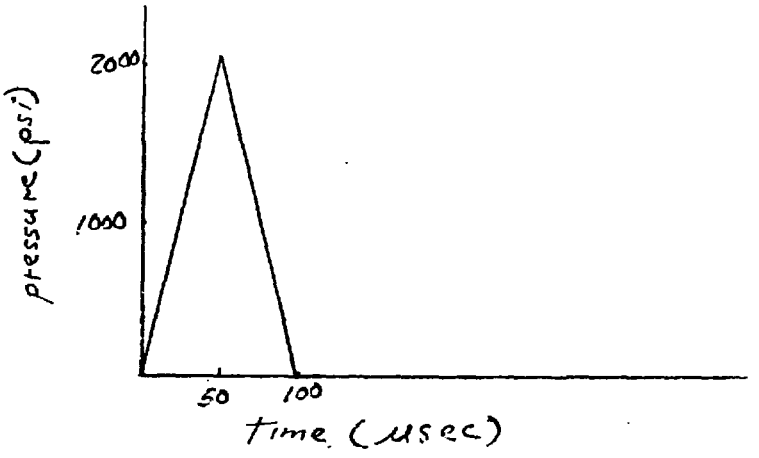

A. Short-duration pressure pulse

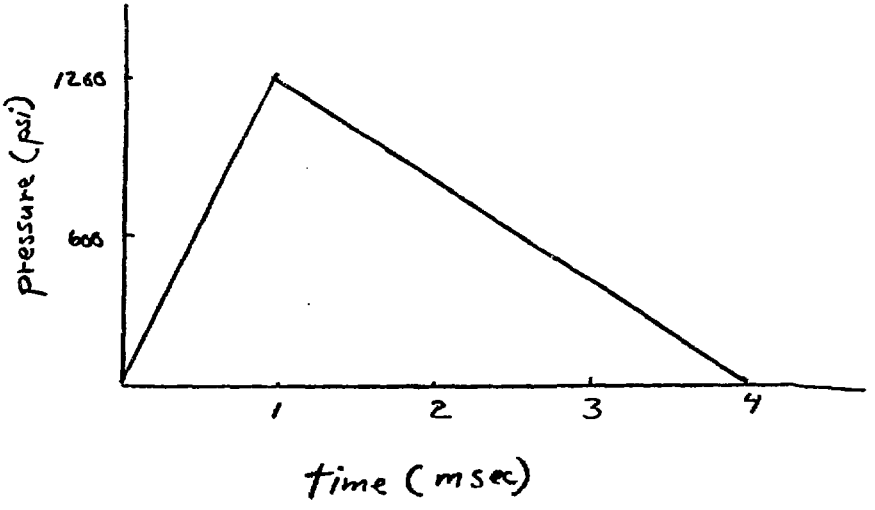

B. Long-duration pressure pulse

Fig. 12. Pressure Pulses

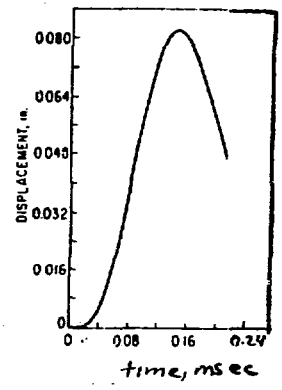

Fig. 13. Normal Displacement History of Flat Midpoint (Short Duration Accident)

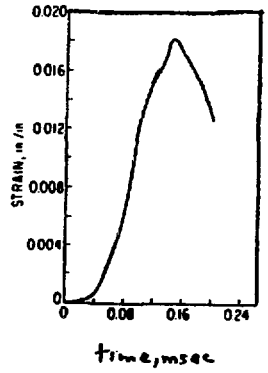

Fig. 14. Strain History of Flat Midpoint on Outside Surface (Short Duration Accident)

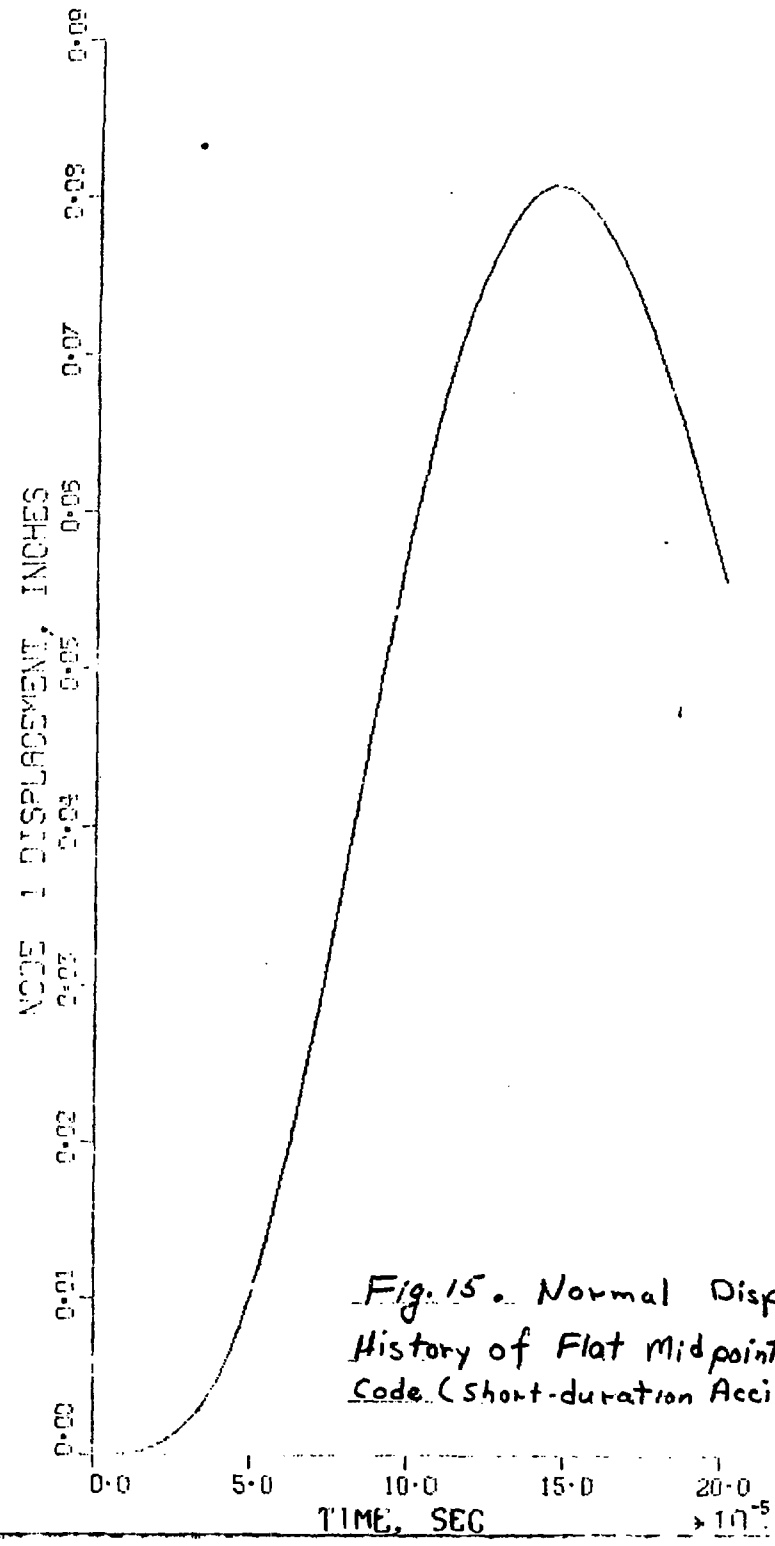

Fig. 15. Normal Displacement History of Flat Midpoint-3D Implicit Code (Short-duration Accident)

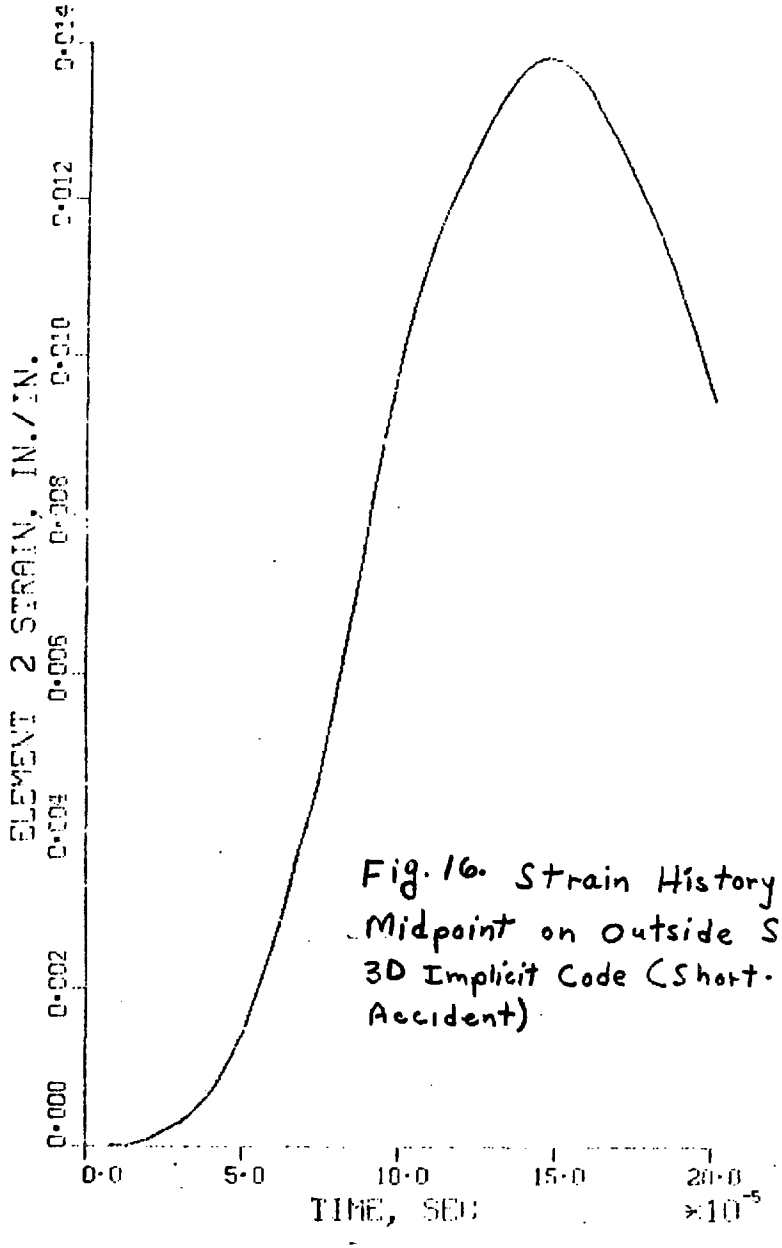

Fig. 16. Strain History of Flat Midpoint on Outside Surface - 3D Implicit Code (Short-duration Accident)

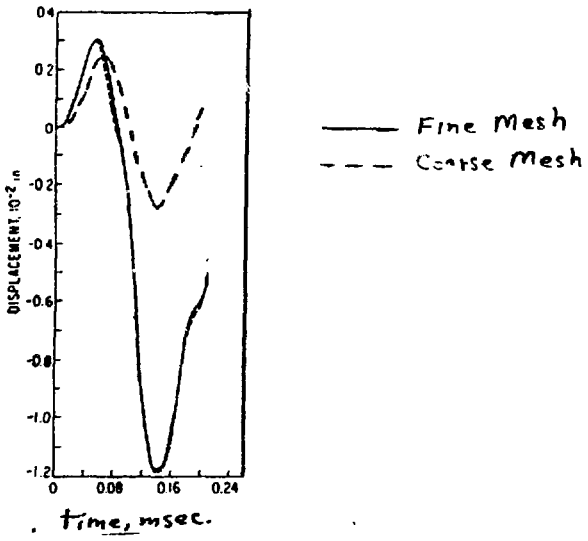

Fig. 17. Normal Displacement History of Corner - STRAW (Short-duration Accident)

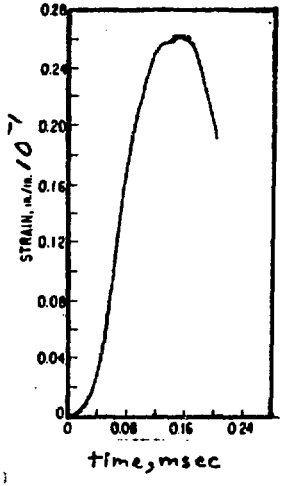

Fig. 18. Strain History of Corner on Inside Surface - STRAW (Short-duration Accident)

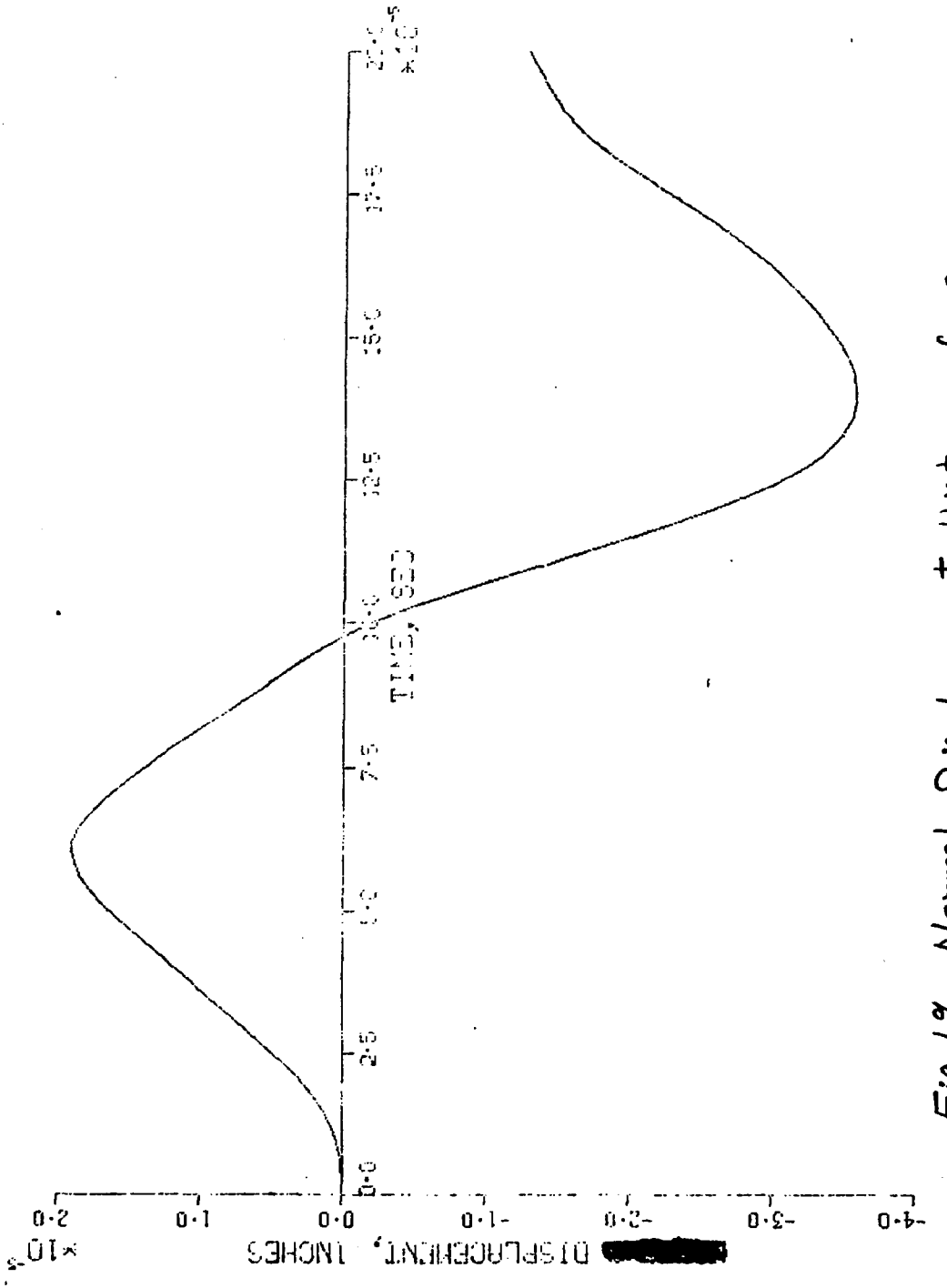

Fig. 19. Normal Displacement History of Corner-3D Implicit (Short-duration Accident)

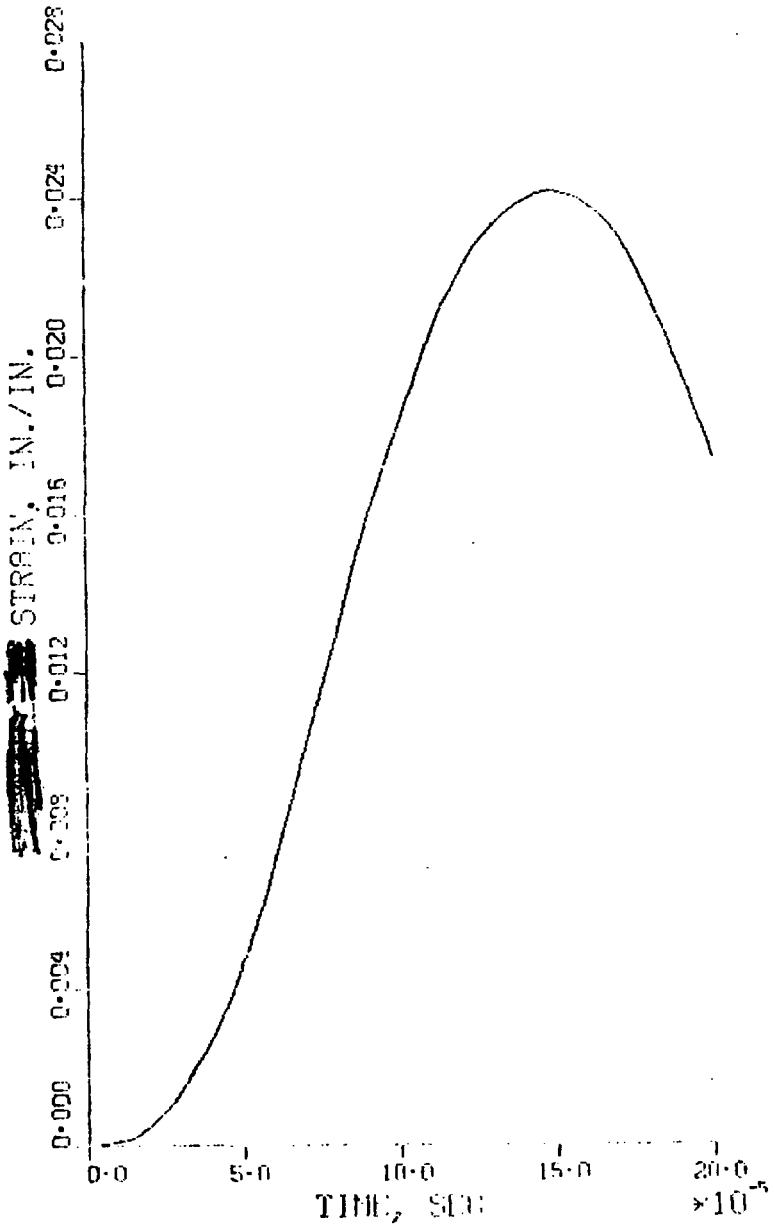

Fig. 20. Strain History of Corner on Inside Surface - 3D Implicit (Short-duration Accident)

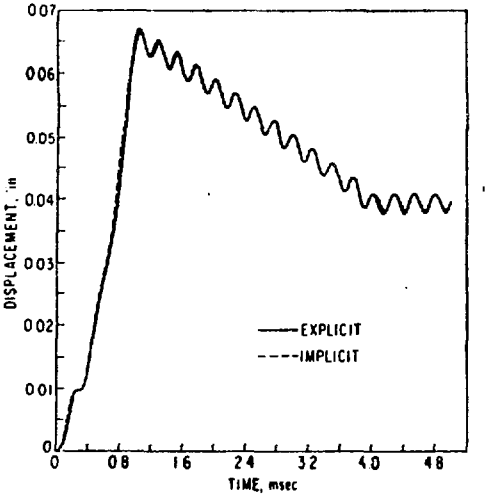

Fig. 21. Normal Displacement History of Flat Midpoint - STRAW (Long-duration Accident)

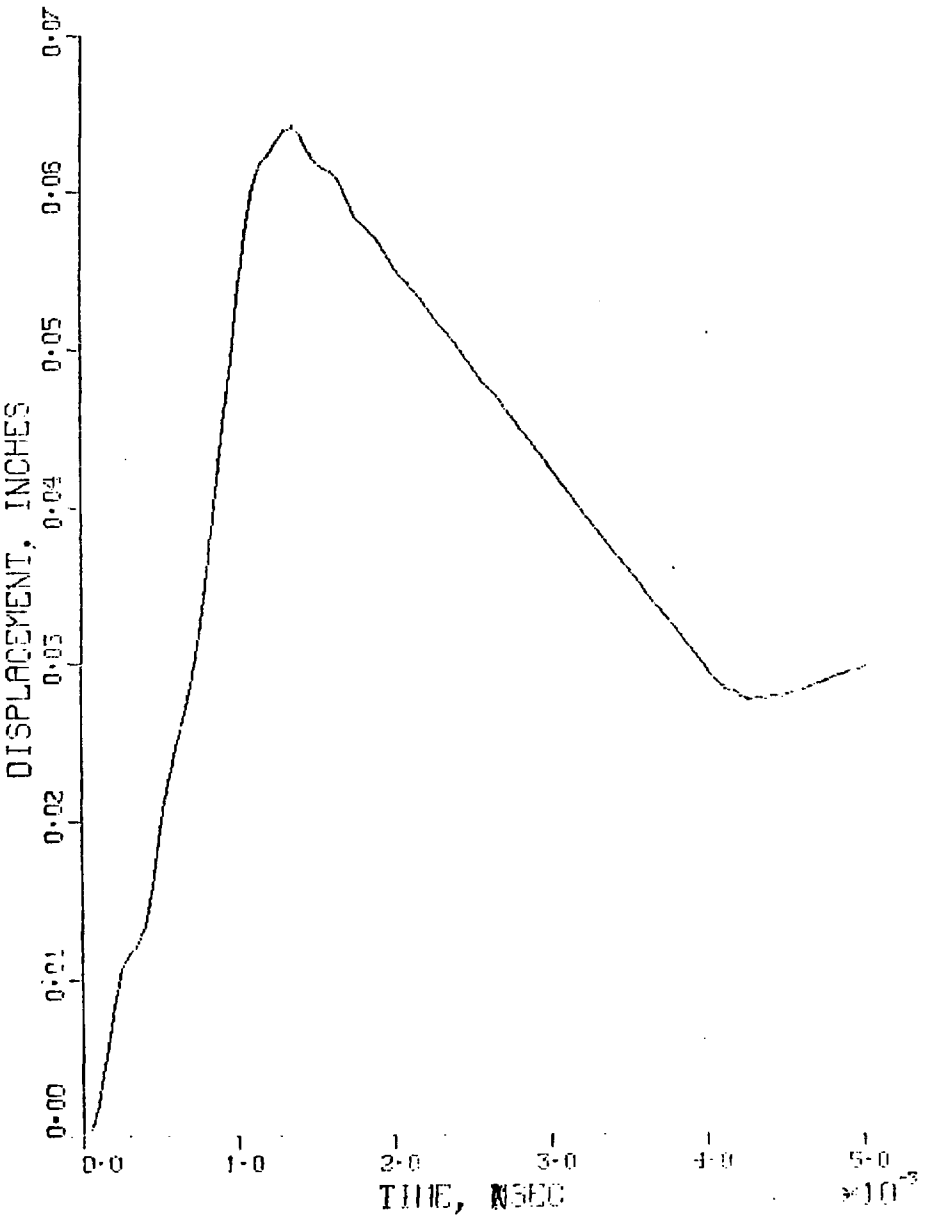

Fig. 22. Normal Displacement History of Flat Midpoint-30-Implicit (Long-duration Accident)

132404 - I MPLICIT - MEM. ΔC = 30 MSEC

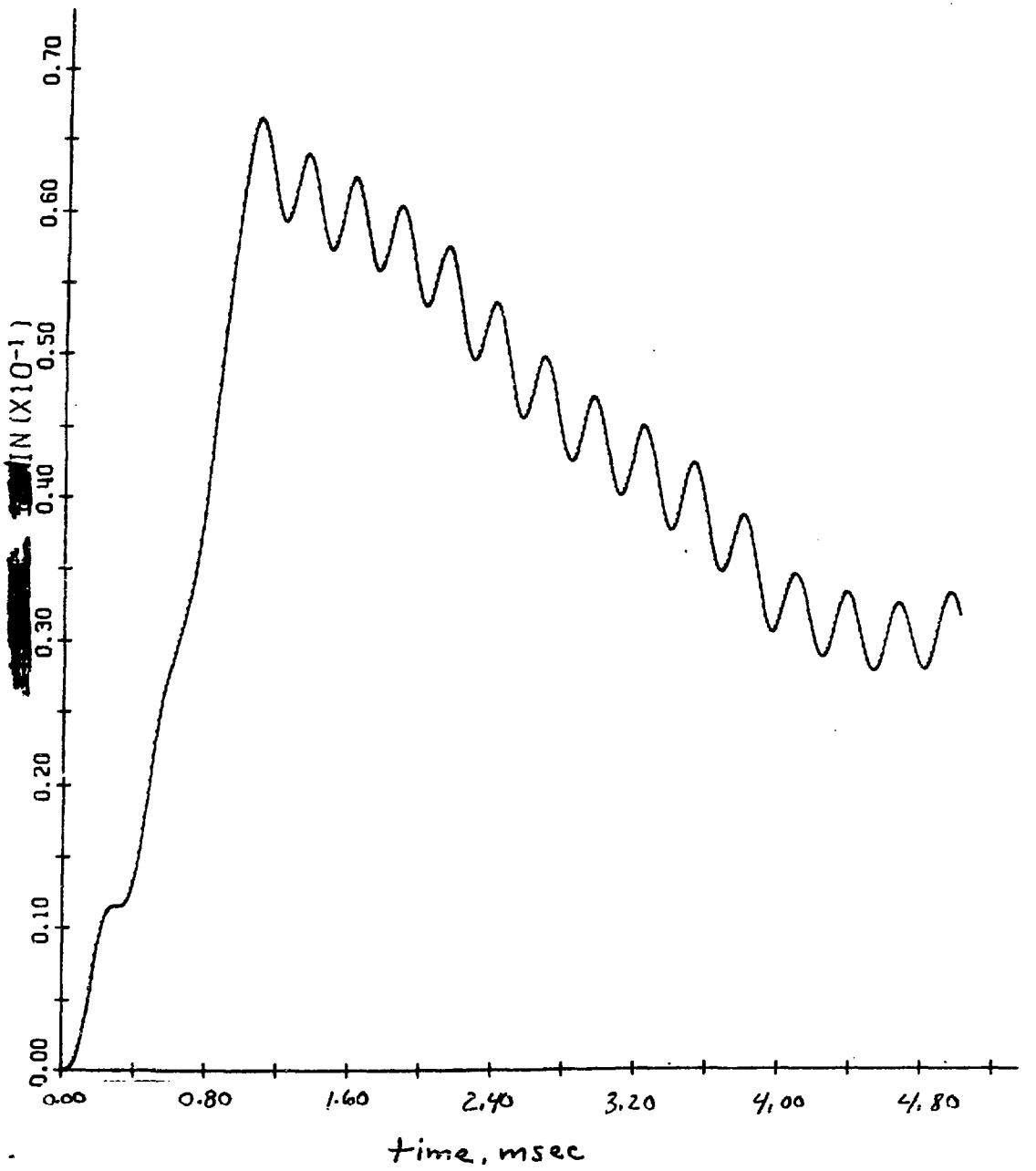

Fig. 23. Normal Displacement History of Flat Midpoint - SADCAT (Long-duration Accident)